

SCIENTIFIC REPORTS



OPEN

Visualization and ligand-induced modulation of dopamine receptor dimerization at the single molecule level

Received: 01 June 2016

Accepted: 23 August 2016

Published: 12 September 2016

Alina Tabor¹, Siegfried Weisenburger^{2,†}, Ashutosh Banerjee¹, Nirupam Purkayastha¹, Jonas M. Kaindl¹, Harald Hübner¹, Luxi Wei², Teja W. Grömer³, Johannes Kornhuber³, Nuska Tschammer¹, Nigel J. M. Birdsall⁴, Gregory I. Mashanov⁴, Vahid Sandoghdar² & Peter Gmeiner¹

G protein-coupled receptors (GPCRs), including dopamine receptors, represent a group of important pharmacological targets. An increased formation of dopamine receptor D₂ homodimers has been suggested to be associated with the pathophysiology of schizophrenia. Selective labeling and ligand-induced modulation of dimerization may therefore allow the investigation of the pathophysiological role of these dimers. Using TIRF microscopy at the single molecule level, transient formation of homodimers of dopamine receptors in the membrane of stably transfected CHO cells has been observed. The equilibrium between dimers and monomers was modulated by the binding of ligands; whereas antagonists showed a ratio that was identical to that of unliganded receptors, agonist-bound D₂ receptor-ligand complexes resulted in an increase in dimerization. Addition of bivalent D₂ receptor ligands also resulted in a large increase in D₂ receptor dimers. A physical interaction between the protomers was confirmed using high resolution cryogenic localization microscopy, with ca. 9 nm between the centers of mass.

Class A G protein-coupled receptors (GPCRs) represent a large family of integral membrane proteins and major pharmacological targets¹ which have traditionally been considered to exist and function as monomers. Biochemical and biophysical evidence has steadily accumulated indicating the ability of GPCRs to assemble as homodimers, heterodimers or higher-order oligomers^{2,3}. A quantitative knowledge of the number and arrangement of protomers, the temporal dynamics of the interaction between monomers, dimers and higher-order oligomers, the effect of receptor ligands on these different conformations, and their pathophysiological roles are of particular interest⁴.

The development of resonance energy transfer (RET) based-techniques such as fluorescence and bioluminescence resonance energy transfer (FRET and BRET) have played an important role in the discovery and characterization of homo- and heteromers in living cells^{2,5–8}. However, these techniques do not provide information about the degree and dynamics of di- and oligomerization at the single molecule level. Recent studies using single-molecule sensitive total internal reflection fluorescence microscopy (TIRF-M) allowed the visualization and tracking of individual GPCRs in the membrane of a living cell in real time^{9–11}. Thus, the dynamics of muscarinic acetylcholine M₁, M₂ and N-formyl peptide receptors, their mobility and dimerization could be observed and quantified by using fluorescent ligands^{9,10,12}. Related work utilized direct labeling of β₁- and β₂-adrenergic receptors with rhodamine-type fluorophores via the SNAP-tag technology^{11,13}. The studies revealed that dimerization of class A GPCRs at the plasma membrane can exhibit a transient equilibrium between dimers and monomers.

¹Department of Chemistry and Pharmacy, Emil Fischer Center, Friedrich-Alexander University, Schuhstraße 19, 91052 Erlangen, Germany. ²Max Planck Institute for the Science of Light and Department of Physics, Friedrich-Alexander University, Günther-Scharowsky-Straße 1/Bldg. 24, 91058 Erlangen, Germany. ³Department of Psychiatry and Psychotherapy, Friedrich-Alexander University, Schwabachanlage 6, 91054 Erlangen, Germany. ⁴The Francis Crick Institute, Mill Hill Laboratory, Mill Hill, London NW7 1AA, UK. [†]Present address: The Rockefeller University, New York, NY 10065, USA. Correspondence and requests for materials should be addressed to P.G. (email: peter.gmeiner@fau.de)

Dopamine D₂-like GPCRs (D_{2L}, D_{2S} and D₃) are associated with several central nervous system diseases including schizophrenia, Parkinson's disease and drug addiction¹⁴. They offer, therefore, an essential and highly important set of drug targets^{15,16}. Recent investigations indicate that D₂-like receptors exist as homomeric^{17–21} or heteromeric complexes^{20,22} and an increased formation of D₂ homodimers was suggested to be associated with the pathophysiology of schizophrenia²³. Targeting of GPCR dimers and ligand-induced modulation of dimerization with selective chemical tools may allow the investigation of the signaling behavior of dimers and the pathophysiology of diseases that are potentially associated with GPCR dimerization. Such compounds may be bivalent ligands incorporating two pharmacophores connected by an appropriate linker that enables simultaneous binding to two adjacent receptor protomers^{24–26}.

In this study, we applied TIRF-M to visualize individual fluorescently labeled dopamine D₂-like receptors in the membrane of living CHO cells using either SNAP-tag technology or fluorescent ligands. This allowed us to study the spatial and temporal organization of the receptors at the single-molecule level under ligand-free and agonist- or antagonist-bound conditions. Furthermore, bivalent D₂-like receptor antagonists²⁷ were synthesized. We could show that these compounds are able to substantially shift the equilibrium between monomers and dimers toward D₂ receptor dimers.

Moreover, we performed nanoscopic distance measurements in order to confirm a physical interaction between the two protomers of SNAP-tagged D_{2L} receptor dimers using cryogenic localization microscopy^{28,29}. This super-resolution microscopy method has recently demonstrated both Angstrom precision and accuracy in resolving nanometer separations. The present study is the first adaptation of this technique to whole cells.

Results

Visualization and transient dimer formation of single SNAP-D_{2L} receptors in the membrane of living cells.

We used TIRF-M to visualize single dopamine receptors in the membrane of living cells. To investigate the spatial and temporal organization of receptor protomers under ligand-free conditions, we employed the SNAP-tag technology¹³. The dopamine D_{2L} receptor was N-terminally labeled with a SNAP-tag, which derives from the O⁶-guanine nucleotide alkyltransferase (ATG). The fusion protein was reacted with a fluorescent benzyl guanine (BG) allowing covalent labeling (Fig. 1a). By investigating cAMP accumulation, the SNAP-D_{2L} receptor was shown to be functionally identical to wild-type D_{2L} receptors (Supplementary Fig. S1f). CHO cells stably expressing the SNAP-D_{2L} receptor were generated with an expression level of 1000 ± 30 fmol mg⁻¹ protein (mean \pm s.e.m.), which is in the range of endogenous expression levels of dopamine receptors *in vivo*³⁰.

To visualize SNAP-D_{2L} receptors in the membrane of stably transfected CHO cells, the cells were specifically labeled with saturating concentrations of Alexa546-BG and imaged by TIRF-M (Supplementary Fig. S1). SNAP-D_{2L} receptors could be identified as individual fluorescent spots moving rapidly in the plasma membrane with a density of 0.67 ± 0.03 spots μm^{-2} (mean \pm s.d., 10 cells), and they were automatically detected and tracked (Fig. 1a,b,d, Supplementary Movie S1). Analysis of the individual receptor spatial trajectories allowed us to calculate their mean squared displacement (MSD) over a range of time intervals (δt) and, hence, to characterize the receptor motion. The linear relationship between MSD and δt showed that receptor diffusion is consistent with a simple Brownian random walk, which is characteristic of free diffusion in the membrane (Fig. 1e). There was no evidence of restricted or anomalous diffusion over the timescale explored in this study (50 ms–3 s). The calculation of the diffusion coefficient from MSD data revealed an average diffusion coefficient (D_{lat}) of 0.084 ± 0.006 $\mu\text{m}^2 \text{s}^{-1}$ (mean \pm s.d., 12031 tracks, 10 cells) for labeled SNAP-D_{2L} receptors, which is similar to the values measured for M₁⁹, β_1 and β_2 ¹¹ receptors (Fig. 1f, Supplementary Table S2). We analyzed the intensity distribution of fluorescent spots observed at the beginning of the video recording (Fig. 1c). The histogram generated from the data was skewed due to the presence of two underlying populations and it was fitted by the sum of two Gaussian functions to estimate the fractions of these populations. The predominant peak (70%) at 197 ± 80 counts pixel⁻¹ (mean \pm s.d.) corresponded to the intensity of single Alexa546-BG molecules on glass slides (Supplementary Note S1, Supplementary Fig. S2) and could be attributed to receptor monomers. The second population (30%, intensity 400 ± 110 counts pixel⁻¹ (mean \pm s.d.)), corresponding to double the intensity of the monomer, and represented receptor dimers. These results are similar to those reported for the M₁ and β_1 receptors^{9,11}.

As controls for the specificity of receptor dimerization observed with the SNAP-D_{2L} receptors and for our labeling, tracking and analysis methods, we used CD86 and CD28 as monomeric and dimeric reference proteins fused with a SNAP-tag at the extracellular N-terminus (SNAP-CD86 and SNAP-CD28) (Fig. 1g,j). We generated stably transfected CHO cell lines of both control constructs which, after labeling with Alexa546-BG and TIRF-illumination, revealed equivalent fluorescent spot densities compared to the stably expressing SNAP-D_{2L} cell line (Supplementary Table S3). Intensity distribution analysis of the fluorescent spots of SNAP-CD86, (Fig. 1g–i), gave a predominant peak with an average intensity of 200 ± 80 counts pixel⁻¹ (mean \pm s.d.) and revealed that $\geq 95\%$ were monomeric, with the remaining existing probably as randomly colocalized spots at a distance below the resolution limit of the system. This provided comfort that the dimer fraction of 30% produced at these levels of expression of SNAP-D_{2L} receptors did indeed reflect a true receptor interaction. To examine whether this approach could detect constitutive dimers, we studied the disulfide-bridged protein dimer SNAP-CD28 (Fig. 1j–l). From the intensity distribution shown in Fig. 1l, it was concluded that 90% of the detected fluorescent spots represent dimers with an intensity of 400 ± 110 counts pixel⁻¹ (mean \pm s.d.) and twice that measured with the monomeric SNAP-CD86. Both control proteins could be tracked with the same accuracy compared to the SNAP-D_{2L} receptor, as determined by calculating the mean trajectory lifetime of each construct which showed no significant differences (Supplementary Fig. S3a,b). These results validated the analytical approach and confirmed the specificity of SNAP-D_{2L} receptor dimerization.

Investigation of cell lines with reduced expression of the SNAP-D_{2L} receptor showed a reduced fraction of dimers (Fig. 2). A density dependent behavior has also been described for β_1 - and β_2 -adrenergic receptors¹¹ and is expected for reversible dimerization.

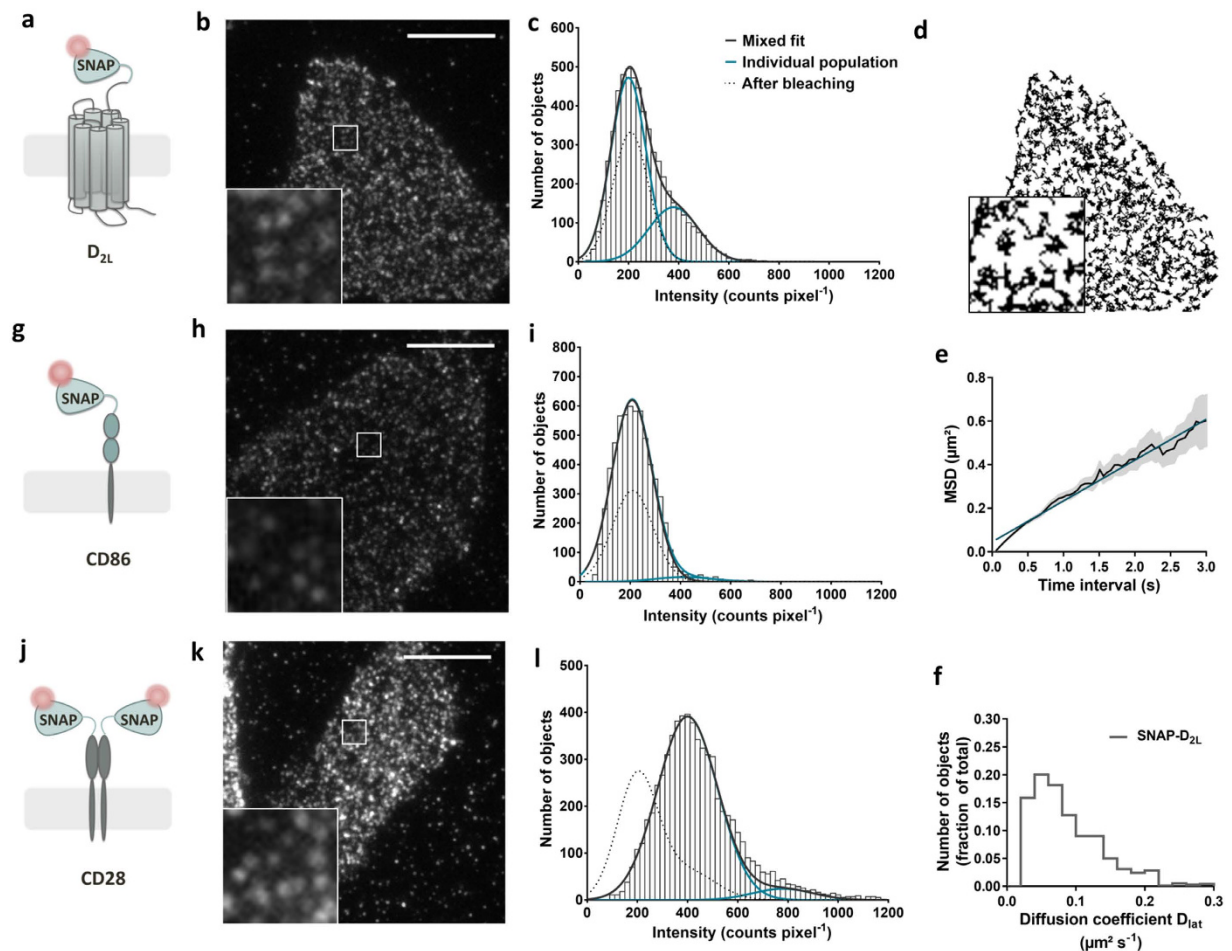


Figure 1. Visualization, tracking and analysis of the dimerization of single SNAP-tagged D_{2L} receptors using SNAP-CD86 and SNAP-CD28 as monomeric and dimeric reference proteins. (a,g,j) Schematic representation of the SNAP-tagged constructs. (b,h,k) Representative images of single CHO cells, stably transfected with the corresponding labeled protein and visualized by TIRF-M. Scale bar, $10\mu\text{m}$. The first 100 frames of the cell in b are shown in Supplementary Movie S1. Inserts correspond to higher magnification images of the areas in the white boxes. (c,i,l) Representative intensity distributions of fluorescent spots identified over the first 10-frame time window of TIRF illumination of CHO cells, stably transfected with the corresponding construct and labeled with Alexa546-BG. Number of identified particles, $n = 5770$ (c), 6252 (f) and 6458 (i). Data were fitted with a mixed Gaussian model. A mixed Gaussian fit after partial photobleaching (dotted line) was used to estimate the intensity of a single fluorescent molecules in each image sequence. (d) Individual trajectories of moving SNAP- D_{2L} receptors were identified from the entire recording of the cell shown in (b). The insert shows a higher magnification that illustrates the random nature of the diffusive process. (e) Representative plot of the average mean square displacement (MSD) (mean \pm s.d.) versus the time interval (δt) for the trajectories shown in (a). The plot is linear ($r^2 = 0.99$ – linear fit (blue)), over a 3-s timescale, which is consistent with receptor movement following a random walk, and it shows no evidence for anomalous diffusive behavior. (f) Distribution of the diffusion coefficients of the receptor particles tracked in (d).

To address the dynamic behavior of SNAP- D_{2L} receptors dimerization, the fluorescence intensities of individual trajectories were visually inspected (Fig. 3a, Supplementary Movie S3). As illustrated in Fig. 3b, we found that intensity doubling was associated with dimer formation within a trajectory arising from two monomers, forming a dimer, followed by the dissociation of the dimer into two monomers. From an analysis of the lifetimes of 120 dimers with trajectories similar to that shown in Fig. 3b, the lifetime of the transient formation of dimers could be shown to be approximately 0.50 s (95% confidence interval: 0.44–0.60) (half-life ($t_{1/2}$) of 0.35 s time (95% confidence interval: 0.31–0.41) (Fig. 3c). We also observed that the rate of receptor diffusion was negatively correlated with the size of receptor complexes (Fig. 3d). As expected, larger dimers diffused more slowly ($0.075 \pm 0.027\mu\text{m}^2\text{s}^{-1}$, $n = 373$ from 3 cells, mean \pm s.d.) compared to the smaller monomers ($0.104 \pm 0.052\mu\text{m}^2\text{s}^{-1}$, $n = 412$ from 3 cells, mean \pm s.d.)³¹, a diagnostic behavior that could be also shown for the monomer and dimer control proteins SNAP-CD86 and SNAP-CD28, respectively (Supplementary Fig. S3d, Supplementary Table S3).

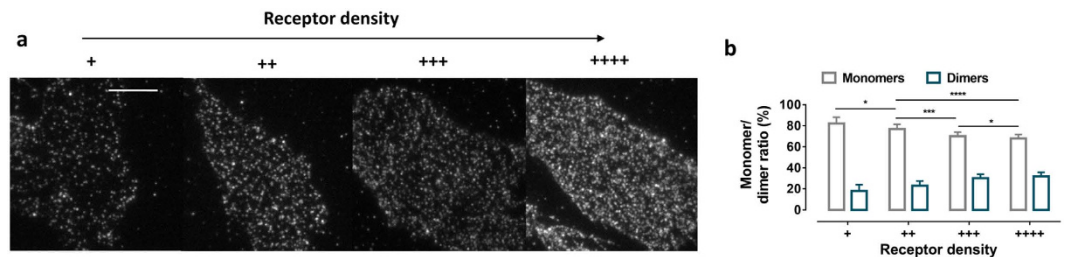


Figure 2. Dependence of the distribution of monomers and dimers on receptor density. (a) Representative receptor density level: + 0.38 ± 0.016 spots μm^{-2} (mean \pm s.d., 8 cells), ++ 0.52 ± 0.039 spots μm^{-2} (mean \pm s.d., 10 cells), +++ 0.67 ± 0.031 spots μm^{-2} (mean \pm s.d., 10 cells), +++++ 0.79 ± 0.046 spots μm^{-2} (mean \pm s.d., 10 cells). (b) The monomer/dimer ratios (mean \pm s.d.) were calculated from the fitted fluorescence intensity distributions of fluorescent ligand receptor complexes using a mixed Gaussian model (compare to Fig. 1c). The statistical significance of the differences in monomer levels in the four groups was determined by an unpaired t-test (* p -value < 0.05, *** p -value < 0.010, **** p -value < 0.0001).

Cryogenic localization microscopy for nanometer distance measurement of two protomers in a SNAP-tagged D_{2L} receptor dimer.

To investigate the physical interaction of two dopamine receptor protomers in a dimer configuration, we applied cryogenic localization microscopy as a super-resolution technique, where the stochastic blinking behavior of the fluorophores was used to distinguish and localize them individually. The method allows nanometer distance measurement with angstrom accuracy^{28,29}. We prepared samples with CHO cells stably expressing SNAP-D_{2L} receptors adhered to clean fused silica cover slides. To increase the adherence of the cells, the cover slides were treated with hydrofluoric (HF) acid prior to a thorough cleaning procedure. We verified that the HF treatment did not influence the diffusion and dimerization of SNAP-D_{2L} receptors (Fig. 4a–d). The samples were then mounted in the vacuum chamber of a flow cryostat and cooled to liquid helium temperature ($T = 4.3$ K). In this experiment (Supplementary Fig. S4 for a schematic drawing of the optical and cryogenic setup), the microscope objective was located outside of the vacuum chamber so that objective-based TIR-illumination was not accessible. Instead, we used a wide-field epi-illumination, which was accompanied by a higher background level caused by out-of-focus fluorescence compared to samples fabricated by spin-coating extremely clean solutions of purified biomolecules. Because of the larger absorption cross-sections of chromophores at cryogenic temperatures this effect is particularly dramatic in our experiment. To address this issue, we reduced the amount of cellular material in the region of interest without affecting the SNAP-D_{2L} receptor diffusion by inducing filopodia tube-like membrane protrusions through exposure of the cells to hypo-osmotic stress conditions (Fig. 4e,h). The direct comparison between wide-field epi-illumination and TIRF-mode for the same CHO cell at room temperature showed that the level of background fluorescence in the membrane protrusion regions is similar (Fig. 4f,g). We thus concentrated our analysis on these regions during the cryogenic measurements. There have been several attempts to deal with higher labeling densities and the resulting overlapping fluorophores, e.g. super-resolution optical fluctuation imaging (SOFI)^{32,33} and the Bayesian localization analysis (Bayesian Bleaching and Blinking, 3B analysis)³⁴. The latter models the complete data set taking into account the number of fluorophores, their positions and their on/off states, and performs a global optimization. This way, blinking fluorophores that reappear at a later, not necessarily adjacent, frame will have an improved localization precision.

We decided to apply the 3B analysis to our data that were recorded at cryogenic temperatures. Figure 5a shows the time-averaged recording of two CHO cells at cryogenic temperatures. A region with membrane protrusions is located between the two cells (white square). Applying the 3B analysis to this region yielded the super-resolution reconstruction image shown in Fig. 5b. The localization precision was determined to be better than 10 nm by analyzing the widths of cross-sections. To extract distance information from our experimental data, we computed pairwise distances from the positions of the fluorophores as determined by the 3B analysis. Figure 5c shows a histogram of the pairwise distances for the SNAP-D_{2L} dopamine receptor (blue). The histogram is corrected by subtracting a simulated histogram which takes into account both an offset caused by random distances due to either background fluorescence mistakenly identified as fluorophores or receptors in a monomeric state as well as the geometry of the membrane protrusions (see Methods). As a control experiment, we looked at CHO cells stably expressing SNAP-CD86 monomers (grey histogram in Fig. 5c). There is a clear peak in the histogram for SNAP-D_{2L} (blue) at 9.1 ± 11.3 nm (mean \pm s.d.) which is not present in the control experiment (grey). The experimentally obtained average distance was thus about 9 nm (Fig. 5d) and is in good agreement with the range of distances between two Alexa546 fluorophores (approximately 3–13 nm) provided from a homology model (Supplementary Fig. S5, Supplementary Note S2).

Specific receptor ligands are able to modulate the monomer-dimer ratio. We investigated whether the ratio between monomers and dimers could be modulated by specific dopamine receptor ligands. Chemical synthesis of the fluorescently labeled bivalent ligands of type 2 and monovalent agonist and antagonists of types 1, 4 and 5 was achieved starting from the respective pharmacophores that were substituted with an alkyne-functionalized handle (Figs 6a and 7a, Supplementary Fig. S11–S16). Using click chemistry, linker units were introduced by copper-catalyzed azide–alkyne cycloaddition (CuAAC)³⁵. The primary amino groups of the generated triazoles were coupled to Cy3B-NHS ester (which was used because of its excellent photophysical

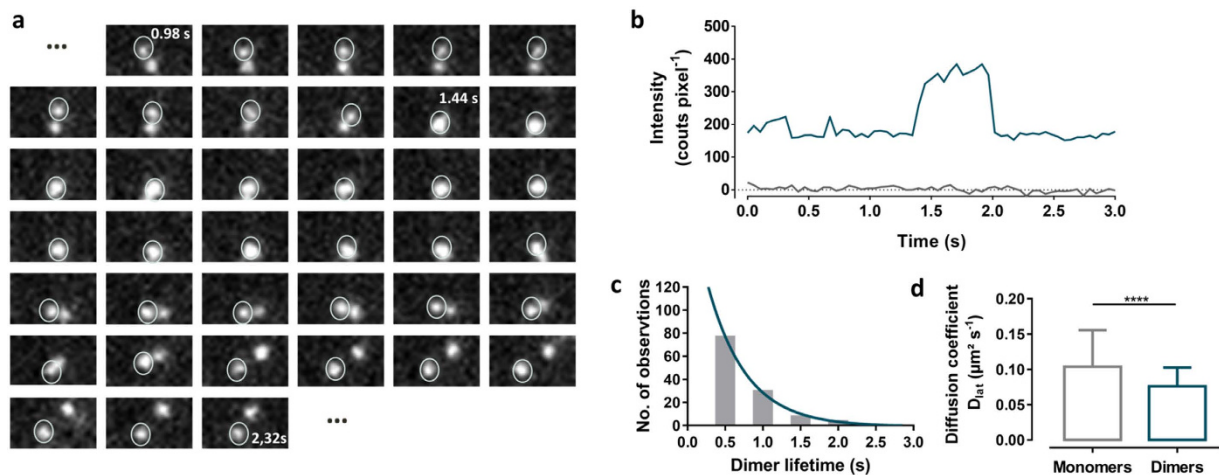


Figure 3. Transient dimer formation of SNAP-D_{2L} receptors. (a) 48 sequential frames of two Alexa546-labeled SNAP-D_{2L} receptors showing transient dimer formation (frame rate of 19.32 fps) (also shown in Supplementary Movie S3). (b) Intensity profile (blue) of the marked fluorescent SNAP-D_{2L} receptor shown in (a), compared to background intensity (grey). (c) A histogram of the lifetimes of 120 SNAP-D_{2L} receptor dimers taken from trajectories similar to those in (a) and collected in 0.5 s bins. The solid line represents a one-phase exponential fit for a mean lifetime of 0.50 s (95% confidence interval: 0.44–0.60). (d) Effect of the size of SNAP-D_{2L} receptors on their lateral diffusion. The diffusion coefficients (D_{lat}) of the analyzed receptor particles (n) are shown (monomers $-0.104 \pm 0.052 \mu\text{m}^2 \text{s}^{-1}$, $n = 412$ from 3 cells and dimers $-0.075 \pm 0.027 \mu\text{m}^2 \text{s}^{-1}$, $n = 373$ from 3 cells. Data represent mean \pm s.d. The difference, determined by an unpaired t-test (**** p -value < 0.0001) is significant and shows that the receptor mobility is negatively correlated with the size of the receptor complexes.

properties) to form the respective ligand-fluorophore conjugates. Non-fluorescent analogs and further control ligands were synthesized employing the same strategy.

Bivalent Ligands. CHO cells stably expressing the SNAP-D_{2L} receptor were incubated with the dopamine receptor antagonist **1a**, incorporating the privileged 1,4- disubstituted aromatic piperazine structure (1,4-DAP)^{36–38}, or its bivalent analogue **2a**, comprising of two pharmacophores calculated of being capable of bridging adjacent binding sites of physically interacting dimers (Fig. 6a)²⁷. In parallel, we synthesized the analogues **1b** and **2b** containing a hydrophilic substituent to improve aqueous solubility (Fig. 6a, Supplementary Figs S11 and S12). A concentration of 10-fold of the K_i value (Supplementary Table S1), which gives 91% receptor occupancy, was used as the labeling concentration for the monovalent and bivalent ligands **1a–c**, **2a–c** and **3a,b**. We observed that the antagonists **1a** and **1b** had no effect on the monomer/dimer ratio nor on the mobility of the SNAP-D_{2L} receptor compared to the ligand-free conditions (Fig. 6b, Supplementary Fig. S6a, Supplementary Table S2). In contrast, the bivalent antagonists **2a** and **2b** increased the fraction of dimers from 30% to 66% and 58%, respectively. The higher extent of dimerization was also reflected in a significantly reduced mobility of the receptor bivalent ligand complexes with an average diffusion coefficient of $0.074 \pm 0.004 \mu\text{m}^2 \text{s}^{-1}$ for **2a** and $0.075 \pm 0.004 \mu\text{m}^2 \text{s}^{-1}$ (mean \pm s.d.) for **2b** compared to $0.087 \pm 0.003 \mu\text{m}^2 \text{s}^{-1}$ and $0.085 \pm 0.004 \mu\text{m}^2 \text{s}^{-1}$ (mean \pm s.d.) for receptor monovalent ligand complexes **1a** and **1b**, respectively (Fig. 6c, Supplementary Fig. S6b, Supplementary Table S2). To confirm a receptor chelating binding mode of the bivalent ligands **2a** and **2b**, a comparative analysis using unsymmetrically substituted analogues²⁷ that are composed of one pharmacophore which is connected via a spacer to structurally similar non-binding motif with a methyl **3a** or cyclohexyl **3b** unit displacing the methoxyphenyl head group was undertaken (Fig. 6a). The observed monomer/dimer ratios (67%: 33%, **3a** and 66%: 34%, **3b**) and average diffusion coefficients ($0.083 \pm 0.004 \mu\text{m}^2 \text{s}^{-1}$ for **3a** and $0.083 \pm 0.005 \mu\text{m}^2 \text{s}^{-1}$ for **3b**, (mean \pm s.d.)) were similar to those observed for the monovalent ligands **1a** and **1b** (Fig. 6b,c).

The results indicate, that the two D₂ binding pharmacophores of the bivalent ligands **2a** and **2b** are essential and confirm a bivalent, receptor-bridging binding mode, which was also observed in cell lines with a lower SNAP-D_{2L} expression level ($0.52 \pm 0.039 \mu\text{m}^2 \text{s}^{-1}$, mean \pm s.d.) (Supplementary Fig. S6c). An increase of the labeling concentration to 100-fold of the K_i value of the monovalent and bivalent ligands, **1a,b** and **2a,b** respectively, did not have any further effects on SNAP-D_{2L} receptor dimerization and mobility (Supplementary Table S2).

The receptor bridging binding mode of the bivalent ligand **2a** was further verified by the determination of the colocalization time of the two receptors in a dimer. Using SNAP-D_{2L} receptor expressing cells, we recorded the time period from the beginning of the image acquisition and particle tracking in the presence and absence of the monovalent **1a** and bivalent **2a** ligands. The data were compared to those obtained from the monomeric and dimeric SNAP-control constructs (Fig. 6d–i). The observed mean apparent colocalization lifetime, τ , obtained by fitting the data to an exponential decay was 1.16 s (95% confidence interval: 1.10–1.23) which is almost identical to that of the dimeric control protein SNAP-CD28 1.21 s (95% confidence interval: 1.17–1.26). The τ -values for the ligand free SNAP-D_{2L} receptor and for the SNAP-D_{2L} receptor incubated with the monovalent ligand **1a** were estimated to be 0.46 s (95% confidence interval: 0.41–0.51) and 0.42 s (95% confidence interval: 0.35–0.52),

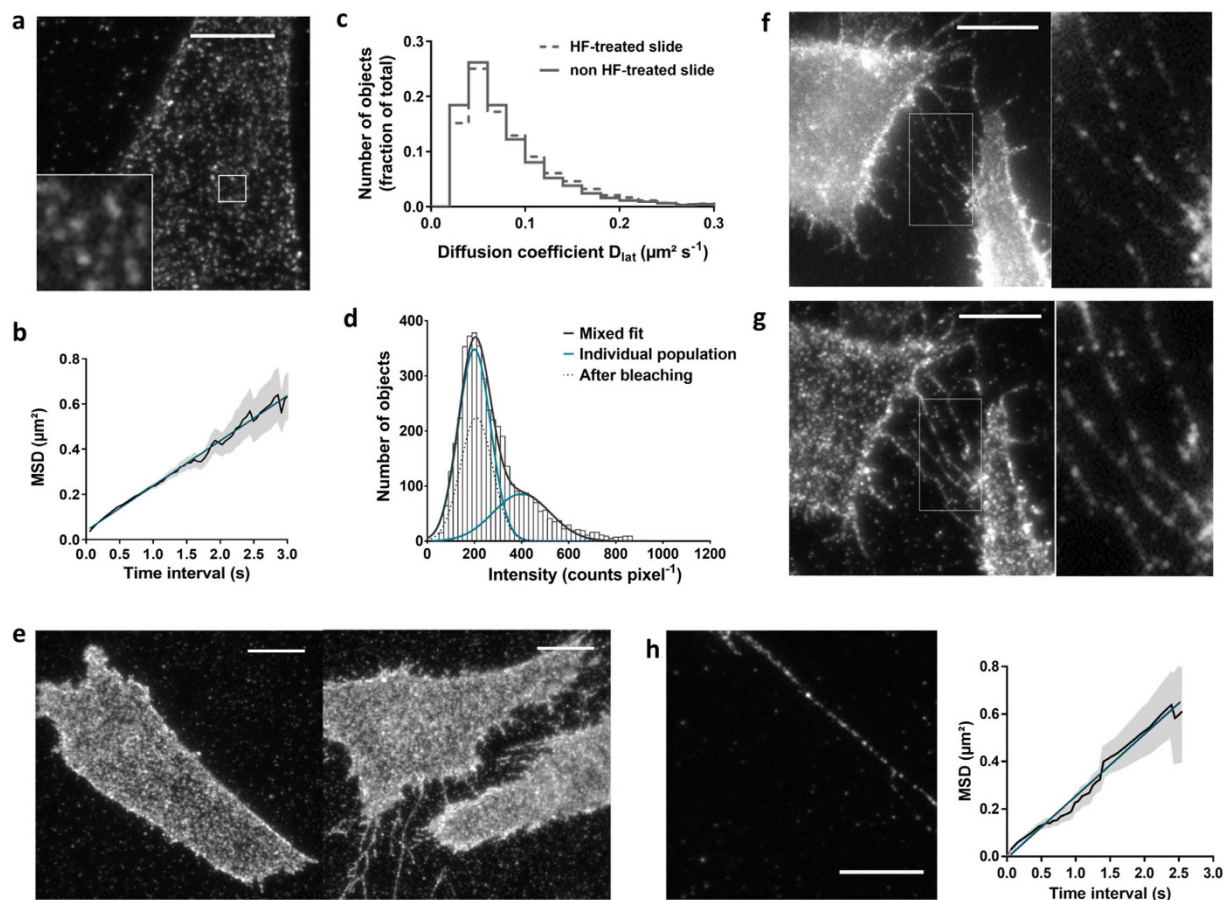


Figure 4. Visualization, diffusion and dimerization of Alexa546-labeled SNAP- D_{2L} receptors and on membrane protrusions using HF-treated slides. (a) Representative images of a single CHO cell stably expressing the SNAP- D_{2L} receptor and seeded on HF-treated glass slides, labeled with Alexa546-BG and visualized by TIRF-M. The insert corresponds to higher magnification image of the area in the small white box. (b) Plot of mean square displacement (MSD \pm s.d.) versus the time interval (δt) of receptor particles that were tracked in a. The plot is linear ($r^2 = 0.99$ – linear fit (blue)), over a 3-s timescale, which is consistent with receptor movement following a random walk. (c) The distribution of the diffusion coefficients of the analyzed receptor particles (n) are shown ($n = 4409$, 5 cells - HF-treated slide; $n = 4409$, 8 cells - non HF-treated slide) and revealed no evidence for anomalous diffusive behavior as a result of HF-treatment. (d) Representative intensity distribution of fluorescent spots identified over the first 10-frame time window of TIRF-illumination. Data were fitted with a mixed Gaussian model (sum of two Gaussian functions). (e) Representative TIRF-M images of CHO cells stably transfected with SNAP- D_{2L} receptor, incubated in iso-osmotic (300 mOsm) (left) and hypo-osmotic PBS (108 mOsm) (right) for 2 h and labeled with Alexa546-BG. (f,g) Imaging of a region of membrane protrusions of CHO cells stably transfected with the SNAP- D_{2L} receptor, incubated in hypo-osmotic (108 mOsm) PBS for 2 h and labeled with Alexa546-BG in epi-illumination (f) and TIRF-illumination (g). (h) Representative images of one membrane protrusion of a CHO cell stably expressing the labeled SNAP- D_{2L} receptor and visualized by TIRF-M. (i) Plot of mean square displacement (MSD \pm s.d.) versus the time interval (δt) of receptor particles that were tracked in (h). The plot is linear ($r^2 = 0.99$ – linear fit (blue)), over a 2.5-s time scale and the calculation of the average diffusion coefficient D_{lat} of $0.077 \pm 0.007 \mu\text{m}^2 \text{s}^{-1}$ (mean \pm s.d., 16 regions of membrane protrusions of 8 cells) revealed no evidence for anomalous diffusive behavior in the membrane protrusions. Scale bars, 10 μm .

respectively, which differs from the τ -value for the monomeric control protein SNAP-CD86 of 0.22 s (95% confidence interval: 0.20–0.25) which is associated with random colocalization of protein molecules. The data are thus compatible with the receptor dimer being stabilized by the bivalent ligand **2a** during the complete image acquisition time.

To estimate the lifetime of the receptor binding mode of the bivalent ligand, we extended our approach by labelling the D_{2L} receptor with the monovalent and bivalent fluorescent ligands **1c** and **2c**. This allowed us to measure the dissociation kinetics of the ligand by direct live cell dissociation experiments (for single molecule characterization of the fluorescent monovalent ligand **1a** and bivalent ligand **2b**, see Supplementary Note S3, Supplementary Fig. S7).

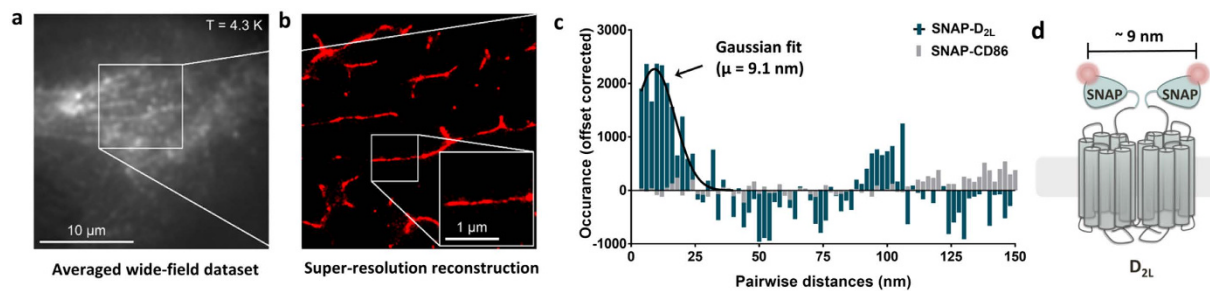


Figure 5. Cryogenic localization microscopy of SNAP- D_{2L} receptor dimers. **(a)** Averaged wide-field dataset of a recording of a CHO cell stably expressing labeled SNAP- D_{2L} . **(b)** Super-resolution reconstruction after 3B analysis of the area indicated by the white square in **(a)**. **(c)** Histogram of the pairwise distances calculated from the emitter positions of the SNAP- D_{2L} (blue) and SNAP-CD86 monomers (gray). The Gaussian fit determines the separation of the SNAP- D_{2L} protomers to be $\mu = 9.1 \pm 11.3$ nm. **(d)** Schematic representation of an Alexa564-labeled SNAP- D_{2L} receptor dimer detected by cryogenic localization microscopy.

CHO cells stably expressing the SNAP- D_{2L} receptor were preincubated for 60 min with the fluorescent monovalent ligand **1c** (Supplementary Fig. S8a) or the bivalent ligand **2c** with a labeling concentration of 10-fold K_i , rapidly washed and further incubated for different periods of time in the presence of 5×10^{-6} M spiperone. As depicted in Supplementary Fig. S8b, the binding of both fluorescent ligands decreased exponentially. The monovalent ligand **1c** dissociated with half-life time $t_{1/2}$ of 19.2 ± 0.6 min (mean \pm s.e.m.) ($\tau = 27.6$ min (95% confidence interval: 23.6–31.6 min) whereas the bivalent ligand **2c** dissociated two fold slower with a $t_{1/2}$ of 38.2 ± 2.0 min (mean \pm s.e.m.) ($\tau = 55.2$ min (95% confidence interval: 47.6–62.7). These results indicate a very slow dissociation rate for type **1** and type **2** ligands.

The dissociation curves verified that during the image acquisition the dissociation of the monovalent and bivalent ligands was negligibly small, which otherwise could have affected the estimates of the monomer/dimer ratios.

Using fluorescent ligands enabled us to monitor non-tagged D_{2L} receptor molecules. A CHO cell line stably expressing D_{2L} receptors at 1041 ± 15 fmol mg^{-1} protein (mean \pm s.e.m.), a level which is similar to the SNAP- D_{2L} cell line, was used. Labeling of the SNAP- D_{2L} and wild type D_{2L} receptor with the monovalent fluorescent ligand **1c** at a concentration representing 10-fold K_i showed fluorescent spot densities similar to the SNAP- D_{2L} receptor labeled with Alexa546-BG, indicating >90% labeling of the receptors by **1c** (Fig. 7, Supplementary Table S2, Supplementary Movie S4). The results of intensity distributions of monomers:dimers (74% : 26%, SNAP- D_{2L} labeled with **1c** and 71% : 29%, D_{2L} labeled with **1c**) suggest that the extent of dimerization was not influenced by the SNAP-tag (Fig. 7c,f).

To verify specific labeling of the D_{2L} receptors with the ligands **1c** and **2c**, CHO cells stably expressing SNAP- D_{2L} receptors were pretreated with 10 μ M spiperone. Only a small number of stationary spots were found, adhered to the glass slide surface (nonspecific binding), but cell labeling was completely blocked and no moving fluorescent spots were observed at the plasma membrane (Fig. 7e).

An intensity distribution analysis to calculate the monomer/dimer ratio of D_{2L} receptors tagged with the bivalent fluorescent ligand **2c** was not possible, since this approach requires labeling of the receptor with a second fluorophore. Nevertheless, the low average diffusion coefficient $0.074 \pm 0.016 \mu m^2 s^{-1}$ (mean \pm s.d., 6 cells) of D_{2L} receptors labeled with the bivalent ligand **2c** provided evidence for increased receptor dimerization (Supplementary Table S2).

Agonists and Antagonists. We chose fluorescent ligands to investigate the effect of agonists on dopamine receptor dimerization compared to antagonist-bound receptors. Accordingly, we designed and synthesized the fluorescent dopamine D_2 receptor antagonists **4a,b** bearing a 1,4-disubstituted phenylpiperazine head group (1,4-DAP), a lipophilic, heterocyclic appendage for enhancing ligand affinity, an ω -amino acid-based linker of different lengths (6 and 16 atoms) and the fluorophore Cy3B (Fig. 8a, Supplementary Figs S13 and S14). The fluorescent agonists **5a,b** shared the same architecture (Fig. 8a) except the 1,4-DAP pharmacophore was replaced by that of the strong D_2 agonist (S)-5-OH-DPAT (Fig. 8a, Supplementary Figs S15 and S16). **5a** and **5b** were potent agonists at the D_{2L} receptor (Supplementary Fig. S9b). The fluorescent ligands of type **4** and **5** were assessed for dopamine receptor affinity using radioligand binding studies, exhibiting low nanomolar to subnanomolar K_i values at the dopamine D_{2L} receptor (Supplementary Table S1). These four fluorescent ligands (**4a,b** and **5a,b**) were characterized on glass slides for their single molecule behaviour and were visible by TIRF-illumination as discrete fluorescent spots. The observed time traces of one-step photobleaching confirmed that single fluorescent m were imaged. The fluorescent intensity distribution of individual spots of these particular fluorescent ligands showed a predominant peak with an average intensity of approximately 200 counts $pixel^{-1}$ (199 ± 78 counts $pixel^{-1}$ **4a**, 190 ± 81 counts $pixel^{-1}$ **4b**, 200 ± 79 counts $pixel^{-1}$ **5a**, and 197 ± 80 counts $pixel^{-1}$ **5b** (mean \pm s.d.)) (compare with Supplementary Fig. S7a,b). CHO cells stably expressing the D_{2L} receptor were incubated with a 10-fold concentration of the K_i value of the corresponding fluorescent ligand **4a,b** and **5a,b** and were imaged by TIRF-M with equivalent photobleaching behaviour (Supplementary Table S4). To confirm specific labelling of these receptors by the fluorescent ligands **4a,b** and **5a,b**, CHO cells stably expressing D_{2L} were pretreated with 10 μ M spiperone, when no cell-specific labeling and a small number of non-specifically adhered, immobile fluorophores could be identified (Supplementary Fig. S9a).

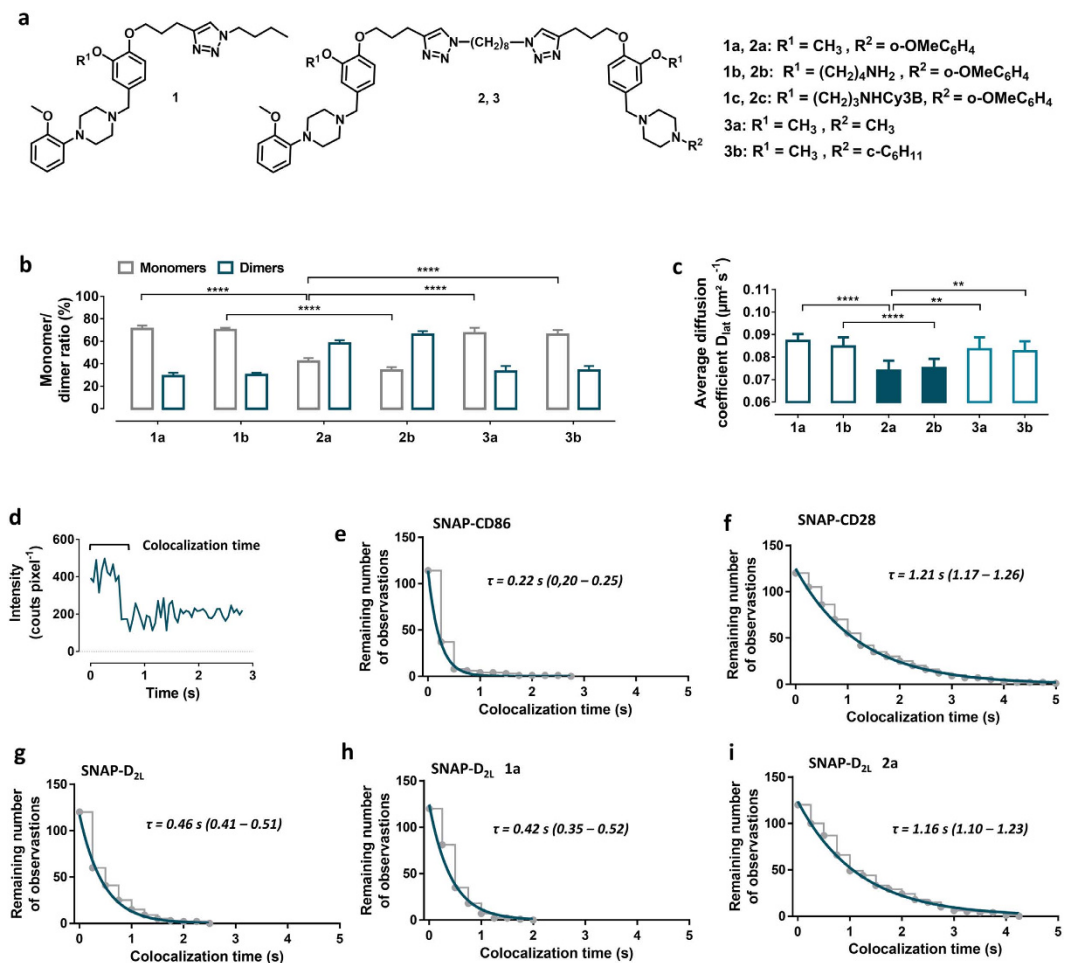


Figure 6. Influence of monovalent (1a,b), bivalent (2a,b) and bivalent control (3a,b) dopamine D_2 receptor antagonists on receptor dimerization. (a) Chemical structures of monovalent ligands (1a–c), bivalent ligands (2a–c), and control ligands (3a,b). (b) Monomer/dimer ratios calculated from fitted fluorescence intensity distributions of Alexa546-labeled SNAP- D_{2L} receptors incubated with monovalent (1a,b), bivalent (2a,b), control (3a,b) ligands using a mixed Gaussian model (Supplementary Table S2, Supplementary Fig. S6a). Data represent mean \pm s.d. of n analysed cells ($n = 16$ for 1a, 8 for 1b, 8 for 2a, 16 for 2b, 6 for 3a and 8 for 3b). (c) Average diffusion coefficients (D_{lat}) of the corresponding ligand-SNAP- D_{2L} receptor complexes of the same analyzed cells in (b). Data in (b,c) represent mean \pm s.d., Statistical analysis was performed by an unpaired t -test (** p -value < 0.01 , **** p -value < 0.0001) and showed that the receptor mobility is negatively correlated with the size of the receptor complexes. (d–g) Comparison of the apparent lifetimes of particle colocalization of the monomeric SNAP-CD86 and dimeric SNAP-CD28 control proteins (e and f respectively) and the SNAP- D_{2L} receptor in the absence and presence of the monovalent ligand 1a or bivalent ligand 2a (g, h, and f respectively). (d) Representative intensity profile of one trajectory which showed intensity doubling from the beginning of the particle tracking followed by one step intensity change which was used to calculate the colocalization time of two particles. (e–i) The apparent lifetime of particle colocalizations (τ ; 95 confidence interval) was calculated by fitting colocalization time data with a one-phase exponential decay function. 120 trajectories like those shown in a were analyzed from 8 different cells in (e), 4 in (f), 6 in (g), 6 in (h) and 4 in (i), respectively.

D_{2L} receptors labeled with the fluorescent antagonist 4a could be identified as individual fluorescent spots moving rapidly on the plasma membrane (Fig. 8b). The intensity distribution of these fluorescent spots showed that the D_{2L} receptor ligand complex (D_{2L} -4a) had a similar pattern to that with the fluorescent antagonist 1c, and contained mainly two populations with the same ratio of monomers (70%) and dimers (30%) (Fig. 8c–f, Supplementary Table S5). Moreover, the average receptor diffusion coefficient, D_{lat} $0.100 \pm 0.009 \mu\text{m}^2 \text{s}^{-1}$ (mean \pm s.d., 18 cells) was similar to that the D_{2L} receptor labeled with the fluorescent antagonist 1c (D_{lat} $0.109 \pm 0.006 \mu\text{m}^2 \text{s}^{-1}$, mean \pm s.d., 6 cells).

The dimer population of the D_{2L} receptors labeled with the fluorescent agonist 5a was increased to 45% from the value of ca. 30% in the presence of antagonist 4a. An identical behavior was observed for the fluorescent ligands with the shorter linkage between the pharmacophore and the fluorophore moieties (42% and 29% for 5b and 4b, respectively) (Fig. 8e,f, Supplementary Table S5).

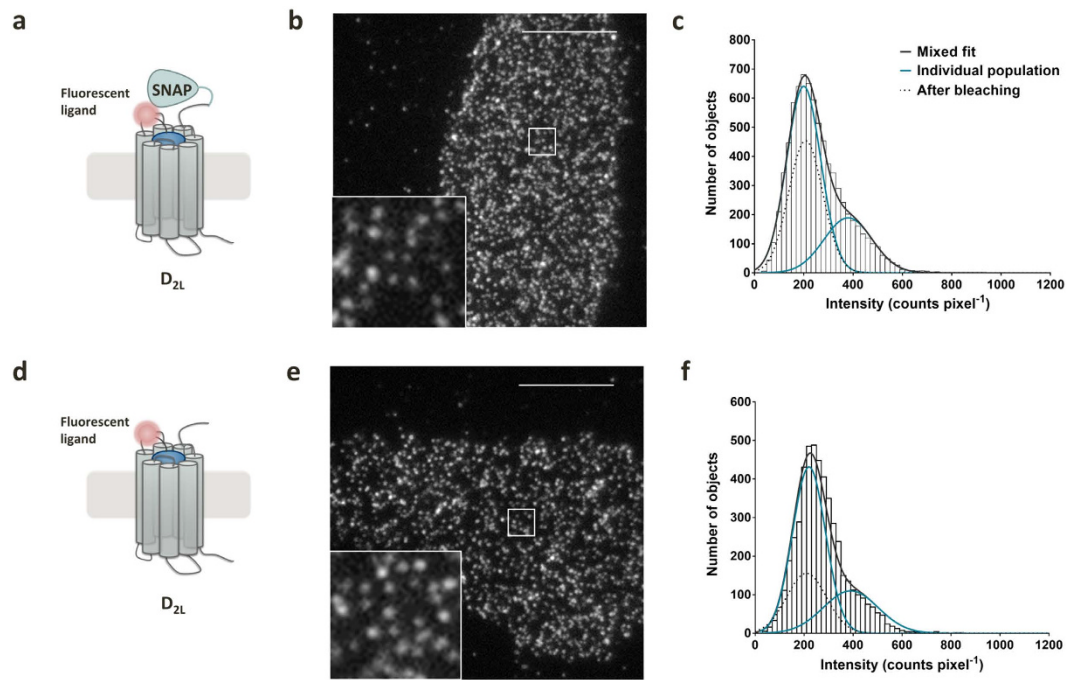


Figure 7. Visualization, tracking and analysis of the dimerization of single SNAP-tagged D_{2L} receptors and wild-type D_{2L} receptors labeled with the fluorescent antagonist 1c. (a,d) Schematic representation of the constructs. (b,e) Representative images of single CHO cells stably transfected with the two constructs, labeled and visualized by TIRF-M. Spot densities were 0.69 spots μm^{-2} (b) and 0.64 spots μm^{-2} (e). Inserts correspond to higher magnification images of the areas in the white boxes. Scale bar, 10 μm . (c,f) Representative intensity distributions of fluorescent spots identified over the first 10-frame time window of TIRF illumination of CHO cells, stably transfected with the corresponding constructs and labeled with the fluorescent ligand 1c (300 nM). Data were fitted with a mixed Gaussian model. A mixed Gaussian fit after partial photobleaching (dotted line) was used to estimate precisely the intensity of a single fluorescent spot in each image sequence.

To investigate if the extent of dopamine receptor dimerization is subtype specific, we extended our strategy to the structurally related human D_{2S} and D₃ receptors. When viewed by TIRF-M, CHO cells stably expressing the D_{2S} or D₃ receptor (receptor expression level (B_{max}) of 970 ± 60 fmol mg^{-1} protein, for D_{2S} and 1060 ± 60 fmol mg^{-1} protein, for D₃, (mean \pm s.e.m.) labeled with the corresponding ligands 4a,b and 5a,b (10-fold K_i value labeling concentration) the labeling pattern appeared similar to CHO cells expressing D_{2L} receptors.

Based on the distribution of individual fluorescent spot intensities of the fluorescent antagonists 4a,b bound to D_{2S} and D₃ receptors, we observed that 18% and 19% of labeled D_{2S} and 10% and 9% of the labeled D₃ receptors form dimers, respectively (Fig. 8e,f, Supplementary Table S5). Agonist labeling with 5a and 5b increased the proportion of dimers and increased the average diffusion rate of all three dopamine D_{2L}, D_{2S} and D₃ receptor subtypes (Fig. 8g, Supplementary Table S5).

The agonist-induced increase in receptor mobility of D_{2L}-5a monomers and dimers is unexpected but might be generated by changes in the conformation of the receptor that influence the mobility or its local environment (Fig. 8h). To confirm this result we incubated Alexa546-labeled SNAP-D_{2L} receptors with the reference D₂ agonist S-(−)-5-OH-DPAT and the antagonist haloperidol. An agonist-induced increase of receptor dimerization and mobility was again observed, whereas the antagonist showed a monomer/dimer ratio that was identical to that of unliganded receptors (Supplementary Fig. S10).

Discussion

We could visualize SNAP-tagged D_{2L} receptors in stably transfected CHO cells under TIRF illumination as individual, freely diffusing fluorescent spots that were evenly distributed at the cell surface. Transient formation of dimers with a lifetime of approximately 0.5 sec and a monomer-dimer ratio of about 70% to 30% was demonstrated, providing evidence that the D_{2L} receptor exists in a dynamic equilibrium between monomers and dimers. These results are consistent with single-molecule studies on other class A GPCRs^{9,11}.

Recent studies have discussed whether the extent and the dynamics of dimerization can be modulated by the absence or presence and the nature of specific ligands^{7,8,21,39,40}. Our data show that the extent of D_{2L} receptor dimerization could be significantly modulated in the presence of dopamine receptor ligands. Treatment with fluorescent agonists, but not antagonists, led to a significant increase of dimers, indicating ligand-specific promotion of attractive protein-protein interactions that determine the equilibrium. The receptor subtypes D_{2S} and D₃ showed an analogous behavior upon antagonist and agonist binding, despite the extent of dimerization being subtype sensitive ($D_{2L} > D_{2S} > D_3$ at an expression level of ca 1 pmol mg^{-1} protein, Supplementary Table S5).

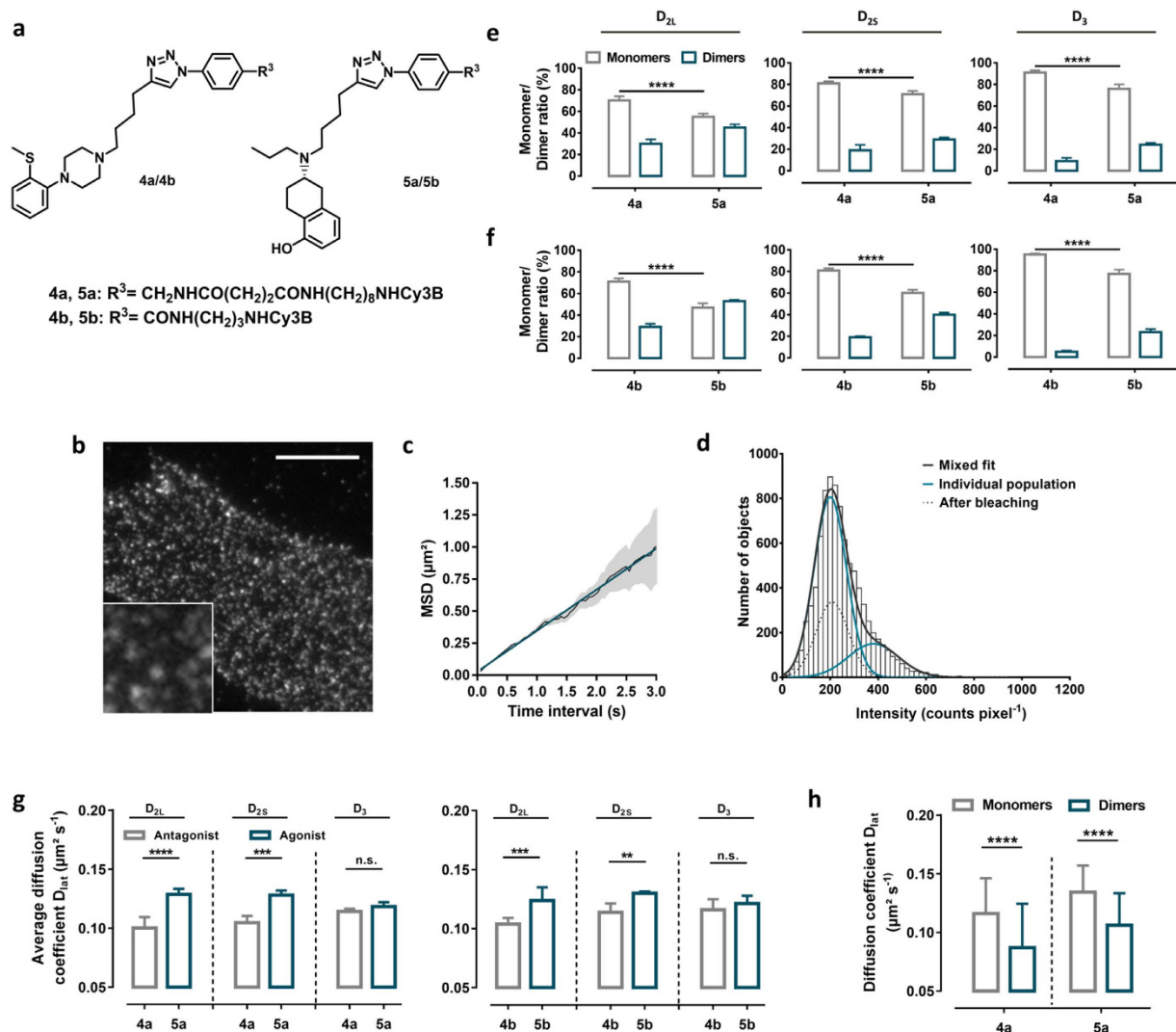


Figure 8. Influence of antagonists (4a,b) and agonists (5a,b) on D_{2L}, D_{2S} and D₃ receptor dimerization. (a) Chemical structures of monovalent fluorescent antagonists (4a,b) and agonists (5a,b). (b) Representative images a single CHO cell stably expressing the D_{2L} receptor, labeled with 4a (38 nM), visualized by TIRF-M. Scale bar, 10 μm. Insert correspond to a higher magnification image of the area in the white box. (c) Plot of average mean square displacement (MSD ± s.d.) versus the time interval (Δt) of the receptor ligand complexes that were tracked (r² = 0.99 – linear fit (blue)). (d) Intensity distribution of fluorescent spots identified over the first 10-frame time window of ligand receptor complex D_{2L}-4a. (e,f) Monomer/dimer ratios of D_{2L}, D_{2S} and D₃ receptors labeled with the fluorescent antagonists 4a,b and agonists 5a,b, calculated from fitted fluorescence intensity distributions of fluorescent ligand receptor complexes using a mixed Gaussian model (compare to (c) and Supplementary Table S5). (g) Average diffusion coefficients (D_{lat}) of the receptor complexes of the same cells analyzed in (e,f). Data in (e–g) represent mean ± s.d. *n* analysed cells (D_{2L}: *n* = 18 for 4a, 19 for 5a, 14 for 4b and 17 for 5b, D_{2S}: 13 for 4a, 12 for 5a, 19 for 4b and 12 for 5b, D₃: 12 for 4a, 13 for 5a, 15 for 4b and 10 for 5b). (e) Representative effects of the size of D_{2L} receptor-ligand complexes on their rates of lateral diffusion. The diffusion coefficient of D_{2L}-4a monomers (0.116 ± 0.030 μm² s⁻¹, *n* = 838 from 3 cells) is greater than that of the dimers (0.087 ± 0.037 μm² s⁻¹, *n* = 185 from 3 cells). This is also found for D_{2L}-5a monomers 0.134 ± 0.023 μm² s⁻¹ (*n* = 1396 from 3 cells) and dimers 0.106 ± 0.027 μm² s⁻¹ (*n* = 558 from 3 cells). Data represent means ± s.d. Statistical analysis was performed by an unpaired *t*-test (***p*-value < 0.01, ****p*-value < 0.001, *****p*-value < 0.0001, n.s. - not significant).

Bivalent ligands that bridge two adjacent protomers display a promising strategy to specifically generate and target GPCR dimers, but their effect on the dynamics and the degree of dimerization is less well established^{124,25}. Our results indicate that bivalent antagonists of type 2 significantly shift the equilibrium towards the dimeric state of D_{2L} with 66% and 58% ligand-dimer complexes being observed in presence of 2a and 2b, respectively. The higher extent of D_{2L} receptor dimerization (ca. 70% of the receptor molecules being present as dimers) was also reflected in a decreased averaged diffusion coefficient of the receptor ligand complexes which is consistent with the increased radius of a dimer compared to the monomer. This indicates a ligand-induced physical interaction

within the D_{2L} receptor dimer, with the decreased average diffusion coefficient of untagged D_{2L} receptors in presence of the fluorescent bivalent ligand providing additional evidence for an increase in dimerization. The effect depends on the presence of two D₂-specific pharmacophores incorporated in the bivalent ligand, because an increase of dimerization was not observed upon the monovalent analogs **1a,b** and the control ligands **3a,b** composed of a pharmacophore with a complete spacer arm and a structurally disordered pharmacophore. Lifetime analysis of the receptor dimers provided evidence that bivalent ligands substantially modulate the lifetime of the investigated D_{2L} receptor dimers. Whereas dimerization has been shown to be a transient phenomenon with a mean lifetime of a dimer of approximately 0.5 s for unliganded receptors and receptors bound by monovalent antagonists, receptors bound to bivalent ligands were stable for longer than the complete tracking time (4 s for the longest tracks). The lifetime of the dimer might be controlled by the dissociation of the ligand, which is in the range of minutes, and not by the dynamics of the protein in the membrane.

Given that homomeric and heteromeric receptor complexes may exhibit unique functional characteristics compared to their constituent receptors and may have a more restricted distribution⁴¹, the ability of ligands to selectively target homomeric dimers in favor of monomeric and heteromeric complexes could have significant therapeutic implications.

The diameter of class A GPCR is approximately 6 nm, around 30-fold lower than the diffraction limit of light⁴². In recent years, the development of super-resolution methods allowed to overcome the diffraction limit and substantially enhanced the optical resolution down to the nanometer scale^{43–45}. To further distinguish between random colocalization of two closely lying receptors and a physical interaction of two protomers in a receptor dimer, we applied cryogenic localization microscopy, a super resolution imaging technique by single-molecule localization at low temperature (4.3 K). After inducing membrane protrusion formation through exposure of the cells to hypo-osmotic stress conditions, SNAP-D_{2L} receptors in intact CHO cells were frozen, using cryo-immobilization which preserved the structures in a near native state and their behavior was compared to monomeric CD86 membrane proteins. The decreased photo-bleaching at lower temperature and the resultant increase of the localization precision is a beneficial side effect of this technique^{28,29,46}.

Cryogenic localization microscopy allowed us to display SNAP-D_{2L} receptor dimers with high resolution and to measure the distance between their centers of mass. The determined distance of about 9 nm indicated a physical interaction of the protomers. The experimental distance is in good agreement with that predicted by a homology model of the dopamine D₂ receptor homodimer which we developed based on the crystal structure of the β₁ adrenergic receptor⁴⁷.

Methods

Organic synthesis and characterization of ligands. Detailed schemes and conditions for the synthesis of the ligands **1b,c**, **2b,c**, **4a,b** and **5a,b** are provided in Supplementary Figs S11 to S16. Detailed methods and characterization for all compounds and precursors are provided in Supplementary Note S4.

Plasmid constructions. A plasmid coding for the N-terminally SNAP-tagged human dopamine D_{2L} receptor (SNAP-D_{2L}) was generated by replacing the β₂AR coding region of a pSNAP_f-β₂ adrenergic receptor (SNAP-β₂AR) (New England Biolabs). The human D_{2L} receptor was PCR amplified using primers designed to add SbfI and XhoI sites to the fragment termini. This was then ligated into the multiple cloning site downstream of SNAP-coding sequence in the plasmid pSNAP_f. The absence of unwanted mutations was confirmed by sequencing. The construct was functional, as shown by radioligand binding and cAMP concentration-response curves. SNAP-CD86 and SNAP-CD28 were generated by exchange of D_{2L} of the SNAP-D_{2L} plasmid against CD86 and CD28, respectively. Plasmids coding for YFP-CD86 (human CD86 - truncated at R277) and CD28-YFP (YFP - F46L_L68V, human CD28 - truncated at R185) were kindly provided by Martin Lohse (Institute of Pharmacology and Toxicology and Bio-Imaging Center, University of Würzburg, Würzburg, Germany). CD86 or CD28 were PCR amplified and ligated into the plasmid pSNAP_f described above.

Generation of stable CHO-K1 cell lines. Chinese hamster ovary cells (CHO-K1) were cultured in DMEM/F-12, supplemented with 10% FCS, 1% penicillin-streptomycin, 2 mM L-glutamine at 37 °C and in the presence of 5% CO₂. For the generation of the stable cell line expressing SNAP-D_{2L}, SNAP-CD86 or SNAP-CD28, CHO-K1 cells seeded in 6-well dishes and grown to 50% confluence were transfected with Mirus TransIT[®]-2020 (MoBiTec), following the manufacturer's protocol. After 48 h, the medium was changed to medium supplemented with 1200 μg ml⁻¹ geneticin G418 (Gibco) to initiate selection of antibiotic-resistant cells. Several resistant clones were isolated by limiting dilution, and characterized for the SNAP-D_{2L} receptor by radioligand saturation experiments. The protein expression of the CD86 and CD28 was validated by TIRF microscopy. For the maintenance of stably transfected cell lines, the concentration of G418 was reduced to 800 μg ml⁻¹ geneticin G418 to prevent the reversion of transfected CHO-K1 cells to a non-transfected state.

Cell culture. Chinese hamster ovary cells (CHO-K1) stably expressing the human dopamine D_{2L}⁴⁸, D_{2S}⁴⁸ receptor, the SNAP-D_{2L} receptor or the SNAP-CD86 and SNAP-28 proteins were maintained in DMEM/F12 medium supplemented with 10% FCS, 2 mM L-glutamine, 1%, penicillin-streptomycin, and 800 μg mL⁻¹ geneticin. Dihydrofolate reductase gene-deficient CHO-K1 cells stably expressing human D₃ receptors (D₃)⁴⁹ were grown in DMEM medium containing 4.5 g L⁻¹ glucose, supplemented with 10% heat-inactivated dialyzed FBS, MEM amino acid supplement, 2 mM L-glutamine and 1%, penicillin-streptomycin. All cells were grown at 37 °C and in 5% CO₂.

Membrane preparation. Membrane preparations were obtained using the methods described previously⁵⁰. In brief, CHO cells stably expressing the D_{2L}, D_{2S}, D₃ or SNAP-D_{2L} were washed with 10 mL ice cold phosphate-buffered saline (PBS, pH 7.4), treated with harvest buffer (10 mM Tris-HCl, 0.5 mM EDTA, 5.4 mM KCl, 140 mM NaCl, pH 7.4), and dissociated using a cell scraper. Subsequently they were pelleted at 200 g for 8 min at 4 °C and resuspended in 10 mL of ice cold homogenate buffer (50 mM Tris-HCl, 5 mM EDTA, 1.5 mM CaCl₂, 5 mM MgCl₂, 5 mM KCl, 120 mM NaCl, pH 7.4). Cell suspensions were then lysed using an Ultraturrax (20000 rpm, 5 times for 5 s) and centrifuged at 50000 g for 15 min. After resuspending the membranes in the binding buffer (50 mM Tris-HCl, 1 mM EDTA, 5 mM MgCl₂, 100 μg mL⁻¹ bacitracin, 5 μg mL⁻¹ soybean trypsin inhibitor, pH 7.4) they were homogenized with a glass–Teflon homogenizer for 7 min at 4 °C. The homogenized membranes were shock-frozen in liquid nitrogen and stored at –80 °C until usage. The protein concentration was determined by the Lowry method⁵¹ using bovine serum albumin as a standard.

Receptor binding studies. Receptor binding studies were carried out as described previously^{27,50,52}. The radioligand [³H]piperone (specific activity 80.6 Ci mmol⁻¹) (Perkin Elmer) was used in saturation experiments to determine the K_d and B_{max} values for the membrane preparations of stably transfected CHO cells expressing the human D_{2L}, D_{2S}⁴⁸, D₃⁴⁹ and SNAP-D_{2L} receptors, respectively. The K_i values for the compounds were obtained by competition experiments. In brief, the assay were carried out in the 96-well plates at protein concentration of 1–8 μg assay⁻¹ tube in a final volume of 200 μL and [³H]piperone at final concentrations of 0.125–0.200 nM for D_{2L}, D_{2S}, D₃ and SNAP-D_{2L} receptors. The K_D values of [³H]piperone for D_{2L}, D_{2S}, D₃ and SNAP-D_{2L} receptors, were 0.053–0.085, 0.067–0.120, 0.095–0.180 and 0.110–0.130 nM respectively, and the corresponding B_{max} values were in the range of 610–640, 1500–4800, 4200–6450 and 2000–2100 fmol mg⁻¹.

Data analysis for receptor binding studies. Analysis of the saturation experiments were performed using a nonlinear regression analysis of the data for the determination of K_D and B_{max} values using PRISM (GraphPad Software). Competition curves were fitted to a sigmoid curve by nonlinear regression analysis in which the log IC₅₀ value and the Hill coefficient were free parameters. IC₅₀ values were transformed to K_i values according to the equation of Cheng and Prusoff⁵³.

Adenylyl cyclase inhibition assay. Bioluminescence based cAMP-Glo™ assays (Promega) were performed according to the manufacturer's instructions. Briefly, CHO cells stably expressing the D_{2L} or SNAP-D_{2L} receptor were seeded into a white half-area 96-well plate (5000 cells well⁻¹) 24 h prior to the assay. On the days of the assays cells were washed with phosphate buffered saline (PBS, pH 7.4) to remove traces of serum and incubated with various concentrations of compounds in the presence of 20 μM forskolin in serum-free medium that contained 500 μM IBMX and 100 μM Ro 20–1724, pH 7.4. After 15 min of incubation at 25 °C cells were lysed with cAMP-Glo lysis buffer, the kinase reaction was performed with a reaction buffer containing PKA and finally an equal volume of Kinase-Glo reagent was added. Bioluminescence was read on a microplate reader Victor³V (Perkin-Elmer). The experiments were performed at least three times per compound.

D_{2L} receptor activation. Ligand-induced activation of the human D_{2L} receptors was studied employing inositol phosphate (IP) accumulation assays as described^{54,55}. Briefly, HEK 293 cells were transiently co-transfected with cDNA encoding for D_{2L} and the hybrid G protein Gα_{q15} (Gα_q protein with the last five amino acids at the C terminus replaced by the corresponding sequence of Gα_i; gift from the J. David Gladstone Institutes). Twenty-four hours after transfection, cells were transferred into 24-well plates. After adding myo-[³H]inositol (specific activity = 22.5 Ci mmol⁻¹, PerkinElmer) and incubation for 15 h, medium was aspirated, the cells were washed with serum-free medium supplemented with 10 mM LiCl, and test compounds 37 °C. Then, cells were lysed by adding 0.1 M NaOH. After neutralization with formic acid, the cell extract was separated by anion-exchange chromatography using an AG1-X8 resin (Bio-Rad) by washing and finally eluting total IP directly into scintillation counting vials. Radioactivity was determined by scintillation counting in a Beckman LS 6500 (Beckman). Data were analyzed by normalizing disintegrations per minute (d.p.m.) values; this was done by setting the data for non-stimulated receptor (buffer) equal to zero and the effect for quinpirole equal to 100%.

Glass slide cleaning. 18 mm no. 1 glass slides (Assistant) were extensively cleaned to remove any background fluorescence. First, they were sonicated in a solution containing 12% Decon 90 for 1 h. After three washes with Milli-Q filtered water, they were further sonicated in a solution of 5 M NaOH for 1 h and were washed again three times with Milli-Q filtered water. Glass slides were then dried followed by sonication in chloroform for 1 h. Cleaned glass slides were dried and stored in 100% ethanol until use.

Labeling and preparation for single-molecule TIRF-M imaging. 24 h before the TIRF-experiment dried and cleaned glass slides were placed in a 12 well plate and were coated by incubation with 20 μg ml⁻¹ fibronectin (Sigma–Aldrich) in sterile PBS for 1 h at 37 °C. After coating, fibronectin was aspirated and the glass surface was rinsed one time with sterile PBS. CHO cells expressing SNAP-D_{2L}, SNAP-CD86, SNAP-CD28, D_{2L}, D_{2S} or D₃ receptors were seeded on coated glass slides in phenol-red-free DMEM/F12 supplemented with 10% FCS and were allowed to adhere overnight at 37 °C and 5% CO₂.

SNAP-tag labeling. Cells were washed two times with phenol red-free DMEM/F12 supplemented with 10% FBS and were labeled 30 min at 37 °C with 1 μM Alexa546-BG (SNAP-Surface® Alexa Fluor® 546; New England Biolabs). Subsequently, cells were washed three times with phenol red-free DMEM/F12 supplemented with 10% FBS, each time followed by 5 min incubation at 37 °C.

For the ligand treatment experiments, the indicated concentration of the corresponding ligand in phenol red-free DMEM/F12 supplemented with 10% FBS were added to stably transfected CHO cells, which were ready for imaging, for 1 h before imaging.

Fluorescent-ligand labeling. Cells were washed two times with phenol red-free DMEM/F12 supplemented with 10% FBS, labeled with a 10-fold K_i value concentration of the corresponding fluorescent ligand (Supplementary Table S1) and incubated (**1c**, **2c** and **4a,b** at 37 °C, 5% CO₂ and **5a,b** at room temperature) for 1 h. Specific labeling of the fluorescent ligands was confirmed by pre-incubation with 10 μM spiperone (a potent non-fluorescent dopamine D₂ receptor antagonist) for 2 h, followed by incubation with fluorescent ligand described above.

Subsequently after labeling, cells were washed three times with phenol red-free DMEM/F12 supplemented with 10% FBS. Glass slides with labeled cells were placed in a custom-built imaging chamber (volume = 500 μL). washed two times with imaging buffer (137 mM NaCl, 5.4 mM KCl, 2.0 mM CaCl₂, 1.0 mM MgCl₂, and 10 mM Hepes, pH 7.4). Finally the imaging chamber was refilled with fresh imaging buffer and mounted immediately on a microscope stage for TIRF-M imaging.

TIRF-M imaging system. Experiments were performed at room temperature (24.0 ± 0.3 °C) on a motorized Nikon TI-Eclipse inverted microscope equipped with a 100x, 1.49 NA oil-immersion objective. Fluorescent dyes were excited using a Nikon D-Eclipse C1 laser box with 561 nm laser for TIRF microscopy. Excitation filter at 561/14 nm employing dichroic long-pass mirror (cut-off wavelength 561 nm) was used. The emitted light was passed through emission bandpass filter 609/54 nm (Semrock Rochester), and was projected onto a water-cooled (Polar Series Accel 250 LC, Thermo Scientific) EM-CCD camera (512 × 512 FT, DU-897, Andor) to -98 °C. The microscope control and image acquisition were performed by the NIS Elements software (Nikon Instruments). To ensure homogenous illumination, only the central quarter of the chip (300 × 300 pixel) was used for imaging analysis. The gain of the EM-CCD camera was set and kept constant at 300, binning at 1 × 1, BitDepth at 14 bits, readout speed at 10 MHz and image sequences (300–500 frames, except 1000 frames for photobleaching experiments) were acquired with an exposure time of 50 ms, resulting in the frame rate of 19.32 fps (frames per second). Under these conditions a representative photobleaching half-life time $t_{1/2}$ of 6.23 ± 0.43 (mean ± s.d.) was determined for Alexa564 labeled SNAP-D_{2L} receptors (Supplementary Fig S3c) The evanescent penetration depth was calculated as ~80 nm.

Data analysis for the TIRF-M imaging. The image analysis procedures have been described in detail previously^{9,56,57}. An automated single particle tracking (ASPT) algorithm⁵⁸ implemented in custom-written software, GMimPro (www.mashanov.uk), was used to identify and track individual fluorescent spots on sequential video frames. ASPT settings used were FWHM300nm, R5, L20, Q10 and C999. Output from this image analysis gave fluorophore centroid positions (with 25 nm precision), integrated fluorophore intensities, total fluorophore number and trajectory lifetime. Spatial trajectories and intensity trajectories (i.e. intensities vs. time) were then further analysed to determine: the lateral diffusion coefficient, D_{lat} , which was derived from averaged mean squared displacement (MSD) versus time interval (δt), the average fluorescent spot density (spot μm⁻²) and distribution across the cell membrane and the intensity distribution of individual fluorescent spots and intensity fluctuation with time as well as the lifetime of colocalization. The D_{lat} was measured for each cell separately and the average value (average D_{lat} , mean ± standard deviation (s.d.)) was calculated for an indicated number of cells. Slow-moving objects $D_{lat} < 0.02 \mu\text{m}^2 \text{s}^{-1}$ were excluded from the analysis and only cells with a mobile trajectory fraction (trajectories with a $D_{lat} > 0.02 \mu\text{m}^2 \text{s}^{-1}$) over 0.75 were used for further analysis. Intensity distributions of fluorescent spots identified over the first 10-frame time window of TIRF illumination were fitted with a sum of Gaussian distributions (with standard deviation proportional to square root of intensity level) using the PRISM routine. The ratio of the areas under the Gaussian curves was calculated to give the percentage of the underlying component⁵⁷. Unpaired two-tailed Student's *t*-tests were used for statistical significance.

Determination of the SNAP-tag labeling efficiency. CHO cells stably expressing the SNAP-D_{2L} receptor were seeded on fibronectin (20 μg ml⁻¹) pre-coated 3.5 cm CELLview™ cell culture dishes with an integrated glass bottom (Greiner, surface treatment TC) with a density of 1 × 10⁵ cells and incubated overnight in phenol-red-free DMEM/F12 supplemented with 10% FBS.

Medium was removed and the cells were labeled with increasing concentrations of Alexa564-BG (0–3 μM) as described above. An adequate amount of randomly chosen cells ($n = 15\text{--}30$) per concentration was imaged by TIRF-microscopy. One image sequences of 5 frames cell⁻¹ was acquired with an exposure time of 50 ms. Further imaging settings were kept identical as described above. Brightfield images were captured and used as a guide for non- or weakly-labeled cells.

Kinetic fluorescent ligand binding studies. For live-cell kinetic experiments to characterize the association and dissociation kinetics of fluorescent ligands, CHO cells stably expressing the SNAP-D_{2L} receptor were prepared as described above for the determination of the SNAP-tag labeling efficiency.

Determination of the association rate. Medium was replaced by fresh DMEM/F12 supplemented with 10% FBS and the fluorescent ligand was added at a concentration representing a 10-fold K_i value. The whole cell fluorescence at 37 °C was measured at times up to 210 min.

Determination of the dissociation rate. Medium was replaced by fresh DMEM/F12 supplemented with 10% FBS and the fluorescent ligand was added at a concentration representing 10-fold K_i value and incubation was continued for 60 min at 37 °C to reach equilibrium binding. Subsequently, the cell culture dishes were placed on

the microscope stage and the incubation medium was replaced by spiperone with a final concentration of 5 μM in imaging buffer. The moment of spiperone addition was considered at $t = 0$ min and bound fluorescent ligand to a whole cell was imaged at multiple time intervals post $t = 0$ min (5 min to 340 min). An adequate amount of cells was imaged at each time interval by TIRF-microscopy.

Calculation of the background corrected mean fluorescence intensity of single cells and analysis.

Calculation of the mean background corrected fluorescence intensity $I(t)$ (arbitrary units) at time t of single cells for live cell kinetic, SNAP-tag labeling efficiency and photobleaching experiments were performed as follows. Regions of interest (ROI) were drawn around the membrane of an individual fluorescent cell (ROI_{cell}) and the background ($\text{ROI}_{\text{background}}$) outside the cell using Fiji software⁵⁷ (Supplementary Fig. S1b). The total mean intensity over the entire cell area ($I(t)_{\text{total cell}}$) and the mean intensity over the background area ($I(t)_{\text{bg}}$) were measured and $I(t)$ were calculated as $I(t) = I(t)_{\text{total cell}} - I(t)_{\text{bg}}$. Data were imported into PRISM and were fitted as stated for each condition by a one-phase association curve for ≥ 11 cells from three independent experiments per condition. The output provided the rate constant (k), the time constant τ (mean fluorescent lifetime) and the half-life time ($t_{1/2}$) defined as k^{-1} and $\ln 2 k^{-1}$, respectively.

Labeling and preparation for cryogenic localization microscopy. Fused silica cover slips ($7.0 \times 7.0 \times 0.2$ mm, UV grade, Siegert Wafer GmbH) were cleaned by sonication using detergents (deionized water and soap “Frosch”), and alternating rinsing with deionized water and sonication in non-halogenated solvents (acetone, ethanol, 2-propanol, in that order) followed by sonication in Piranha solution (1:1 SO_4 and 30% H_2O_2). Afterwards, the cover slips were stored in deionized water before a treatment in 5% hydrofluoric acid (HF) for 5 min in order to increase adherence of the cells to the cover slips. The cover slips were then dried with nitrogen (5N) and again rinsed with deionized water and ethanol before usage.

The clean and dry HF-treated fused silica slides were then coated with fibronectin like the coating procedure described above (Labeling and preparation for single-molecule TIRF-M imaging). CHO cells stably expressing SNAP-D_{2L} and SNAP-CD86 receptors, respectively, were seeded on coated glass slides in phenol-red-free DMEM/F12 supplemented with 10% FCS and were allowed to adhere overnight at 37 °C and 5% CO_2 . Hypoosmotic stress conditions to induce membrane protrusion formation were attained by incubation in hypo-osmotic PBS (108 mOsm) for 2 h at 37 °C and 5% CO_2 . After incubation, the cells were labeled with Alexa546-BG like the SNAP-tag labeling procedure described above. To exclude artefacts from the HF treatment, the above described procedure, but with 20 min in 5% HF to account for slower etching of borosilicate glass compared to fused silica, was applied to 18 mm, no. 1 glass slides (Assistant) (TIRF-M slides) which were employed for TIRF-M control experiments with CHO cells, stably expressing the SNAP-D_{2L} receptor and labeled with Alexa546-BG.

Cryogenic localization microscopy imaging setup. A schematic drawing of the experimental setup is shown in Supplementary Fig. S4. The experiments were performed on a homebuilt epi-fluorescence microscope. A Coherent Sapphire OPSL laser ($\lambda = 532$ nm) was coupled into a polarization maintaining fiber for beam clear up before it was out-coupled and collimated. A 532-10 band pass excitation filter was used for spectral clear up. The polarization was then adjusted using two wave plates, so that the light is circularly polarized before the microscope objective. A wide-field lens ($f = 400$ mm) focused the laser beam via a 4f telescope ($f = 350$ mm) into the backfocal plane of the microscope objective (Zeiss Neofluar 63x LWD, 0.75 NA). A glass wedge at low angle of incidence (about 5°) was used as a beam splitter. The sample is mounted in the vacuum chamber of a liquid helium flow cryostat (Janis ST-500) on a copper cold finger and cooled to liquid helium temperature ($T = 4.3$ K). The laser power was adjusted to about 5 mW before the microscope objective. The fluorescence is detected in epi-mode. A 538 long pass filter is used as detection filter before an $f = 300$ mm lens focuses the light on the EM-CCD camera (Andor iXon 897). Movies were recorded at a frame rate of 20 fps in frame transfer mode with EM gain = 2400.

Data analysis for the cryogenic localization microscopy. The 3B analysis was performed using the ImageJ PlugIn provided by Rosten *et al.*⁵⁹. Relatively large data sets (50×50 px up to 70×70 px, 1000 frames) were processed using default settings and measured values for the PSF FWHM. The analysis ran for >200 iterations to ensure convergence (runtime >7 days on an i7 3.4 GHz workstation).

We then calculated pairwise distances (Euclidian metric) from the identified positions. These histograms were corrected by subtracting a simulated histogram that was constructed in the following way: The same number of emitters was randomly placed on a three-dimensional cylinder of 150 nm diameter⁶⁰ and the accumulated membrane protrusion length. Pairwise distances were then histogrammed after computing a two-dimensional projection.

Dimer modeling. As a starting structure, our recently described homology model of the D₂ receptor based on the D₃ crystal structure was used⁶¹. The Swiss-PdbViewer⁶² was used to place a SNAP protomer (PDB 3KZY) in different positions on the N-terminal side of the D₂ receptor model with its C-terminus allocated to the receptor. Missing residues, including unresolved SNAP residues, four additional linker residues and unresolved N-terminal D₂ residues were modelled manually. The loop was created and refined by means of the Swiss-PdbViewer loop database. The dimer models were generated by superimposing two identical SNAP-D₂ protomers with the crystal structure of the β_1 -AR dimer (PDB 4GPO)⁶³. Subsequently, the resulting dimer models were submitted to energy minimization as described previously⁶¹. The figure was prepared using UCSF Chimera package 1.10⁶⁷.

References

- Pierce, K. L., Premont, R. T. & Lefkowitz, R. J. Seven-transmembrane receptors. *Nature reviews Molecular cell biology* **3**, 639–650 (2002).
- Bouvier, M. Oligomerization of G-protein-coupled transmitter receptors. *Nature reviews Neuroscience* **2**, 274–286 (2001).
- Milligan, G. G protein-coupled receptor dimerization: function and ligand pharmacology. *Mol Pharmacol* **66**, 1–7 (2004).
- Ferre, S., Casado, V., Devi, L. A., Filizola, M., Jockers, R., Lohse, M. J., Milligan, G., Pin, J. P. & Guitart, X. G protein-coupled receptor oligomerization revisited: functional and pharmacological perspectives. *Pharmacol Rev* **66**, 413–434 (2014).
- Milligan, G. & Bouvier, M. Methods to monitor the quaternary structure of G protein-coupled receptors. *FEBS J* **272**, 2914–2925 (2005).
- Pin, J.-P., Neubig, R., Bouvier, M., Devi, L., Filizola, M., Javitch, J. A., Lohse, M. J., Milligan, G., Palczewski, K., Parmentier, M. & Spedding, M. International Union of Basic and Clinical Pharmacology. LXVII. Recommendations for the Recognition and Nomenclature of G Protein-Coupled Receptor Heteromultimers. *Pharmacol Rev* **59**, 5–13 (2007).
- Angers, S., Salahpour, A., Joly, E., Hilairiet, S., Chelsky, D., Dennis, M. & Bouvier, M. Detection of beta 2-adrenergic receptor dimerization in living cells using bioluminescence resonance energy transfer (BRET). *Proc Natl Acad Sci USA* **97**, 3684–3689 (2000).
- Alvarez-Curto, E., Pediani, J. D. & Milligan, G. Applications of fluorescence and bioluminescence resonance energy transfer to drug discovery at G protein coupled receptors. *Anal Bioanal Chem* **398**, 167–180 (2010).
- Hern, J. A., Baig, A. H., Mashanov, G. I., Birdsall, B., Corrie, J. E. T., Lazareno, S., Molloy, J. E. & Birdsall, N. J. M. Formation and dissociation of M1 muscarinic receptor dimers seen by total internal reflection fluorescence imaging of single molecules. *Proc Natl Acad Sci USA* **107**, 2693–2698 (2010).
- Kasai, R. S., Suzuki, K. G., Prossnitz, E. R., Koyama-Honda, I., Nakada, C., Fujiwara, T. K. & Kusumi, A. Full characterization of GPCR monomer-dimer dynamic equilibrium by single molecule imaging. *The Journal of cell biology* **192**, 463–480 (2011).
- Calebiro, D., Rieken, F., Wagner, J., Sungkaworn, T., Zabel, U., Borzi, A., Cocucci, E., Zurn, A. & Lohse, M. J. Single-molecule analysis of fluorescently labeled G-protein-coupled receptors reveals complexes with distinct dynamics and organization. *Proc Natl Acad Sci USA* **110**, 743–748 (2013).
- Nenasheva, T. A., Neary, M., Mashanov, G. I., Birdsall, N. J. M., Breckenridge, R. A. & Molloy, J. E. Abundance, distribution, mobility and oligomeric state of M2 muscarinic acetylcholine receptors in live cardiac muscle. *Journal of Molecular and Cellular Cardiology* **57**, 129–136 (2013).
- Keppler, A., Gendreizig, S., Gronemeyer, T., Pick, H., Vogel, H. & Johnsson, K. A general method for the covalent labeling of fusion proteins with small molecules *in vivo*. *Nature biotechnology* **21**, 86–89 (2003).
- Beaulieu, J.-M. & Gainetdinov, R. R. The physiology, signaling, and pharmacology of dopamine receptors. *Pharmacol Rev* **63**, 182–217 (2011).
- Zhang, A., Neumeier, J. L. & Baldessarini, R. J. Recent progress in development of dopamine receptor subtype-selective agents: potential therapeutics for neurological and psychiatric disorders. *Chem Rev* **107**, 274–302 (2007).
- Davis, K. L., Kahn, R. S., Ko, G. & Davidson, M. Dopamine in schizophrenia: a review and reconceptualization. *Am J Psychiatry* **148**, 1474–1486 (1991).
- Lee, S. P., O'Dowd, B. F., Ng, G. Y., Varghese, G., Akil, H., Mansour, A., Nguyen, T. & George, S. R. Inhibition of cell surface expression by mutant receptors demonstrates that D2 dopamine receptors exist as oligomers in the cell. *Mol Pharmacol* **58**, 120–128 (2000).
- Armstrong, D. & Strange, P. G. Dopamine D2 receptor dimer formation: evidence from ligand binding. *J Biol Chem* **276**, 22621–22629 (2001).
- Guo, W., Urizar, E., Kralikova, M., Mobarec, J. C., Shi, L., Filizola, M. & Javitch, J. A. Dopamine D2 receptors form higher order oligomers at physiological expression levels. *The EMBO journal* **27**, 2293–2304 (2008).
- Pou, C., Mannoury la Cour, C., Stoddart, L. A., Millan, M. J. & Milligan, G. Functional homomers and heteromers of dopamine D2L and D3 receptors co-exist at the cell surface. *J Biol Chem* **287**, 8864–8878 (2012).
- Albizu, L., Cottet, M., Kralikova, M., Stoev, S., Seyer, R., Brabet, I., Roux, T., Bazin, H., Bourrier, E., Lamarque, L., Breton, C., Rives, M.-L., Newman, A., Javitch, J., Trinquet, E., Manning, M., Pin, J.-P., Mouillac, B. & Durroux, T. Time-resolved FRET between GPCR ligands reveals oligomers in native tissues. *Nature chemical biology* **6**, 587–594 (2010).
- Maggio, R., Aloisi, G., Silvano, E., Rossi, M. & Millan, M. J. Heterodimerization of dopamine receptors: new insights into functional and therapeutic significance. *Parkinsonism & Related Disorders* **15**, Supplement 4, S2–S7 (2009).
- Wang, M., Pei, L., Fletcher, P. J., Kapur, S., Seeman, P. & Liu, F. Schizophrenia, amphetamine-induced sensitized state and acute amphetamine exposure all show a common alteration: increased dopamine D2 receptor dimerization. *Molecular brain* **3**, 25 (2010).
- Hiller, C., Kühhorn, J., Gmeiner, P. & Class, A. G-protein-coupled receptor (GPCR) dimers and bivalent ligands. *Journal of medicinal chemistry* **56**, 6542–6559 (2013).
- Shonberg, J., Scammells, P. J. & Capuano, B. Design strategies for bivalent ligands targeting GPCRs. *ChemMedChem* **6**, 963–974 (2011).
- Hubner, H., Schellhorn, T., Gienger, M., Schaab, C., Kaendl, J., Leeb, L., Clark, T., Moller, D. & Gmeiner, P. Structure-guided development of heterodimer-selective GPCR ligands. *Nat Commun* **7** (2016).
- Kuhhorn, J., Hubner, H. & Gmeiner, P. Bivalent dopamine D2 receptor ligands: synthesis and binding properties. *Journal of medicinal chemistry* **54**, 4896–4903 (2011).
- Weisenburger, S., Jing, B., Hanni, D., Reymond, L., Schuler, B., Renn, A. & Sandoghdar, V. Cryogenic colocalization microscopy for nanometer-distance measurements. *Chemphyschem: a European journal of chemical physics and physical chemistry* **15**, 763–770 (2014).
- Weisenburger, S., Jing, B., Renn, A. & Sandoghdar, V. Cryogenic localization of single molecules with angstrom precision. *Proc. SPIE 8815, Nanoimaging and Nanospectroscopy* **8815**, 88150D–88150D-9 (2013).
- Boyson, S. J., McGonigle, P. & Molinoff, P. B. Quantitative autoradiographic localization of the D1 and D2 subtypes of dopamine receptors in rat brain. *The Journal of neuroscience: the official journal of the Society for Neuroscience* **6**, 3177–3188 (1986).
- Saffman, P. G. & Delbruck, M. Brownian motion in biological membranes. *Proc Natl Acad Sci USA* **72**, 3111–3113 (1975).
- Dertinger, T., Colyer, R., Iyer, G., Weiss, S. & Enderlein, J. Fast, background-free, 3D super-resolution optical fluctuation imaging (SOFI). *Proc Natl Acad Sci USA* **106**, 22287–22292 (2009).
- Dertinger, T., Heilemann, M., Vogel, R., Sauer, M. & Weiss, S. Superresolution Optical Fluctuation Imaging with Organic Dyes. *Angew Chem Int Edit* **49**, 9441–9443 (2010).
- Cox, S., Rosten, E., Monypenny, J., Jovanovic-Talman, T., Burnette, D. T., Lippincott-Schwartz, J., Jones, G. E. & Heintzmann, R. Bayesian localization microscopy reveals nanoscale podosome dynamics. *Nat Methods* **9**, 195–200 (2012).
- Rostovtsev, V. V., Green, L. G., Fokin, V. V. & Sharpless, K. B. A stepwise Huisgen cycloaddition process: Copper(I)-catalyzed regioselective “ligation” of azides and terminal alkynes. *Angew Chem Int Edit* **41**, 2596–+ (2002).
- Löber, S., Hübner, H., Tschammer, N. & Gmeiner, P. Recent advances in the search for D3- and D4-selective drugs: probes, models and candidates. *Trends Pharmacol Sci* **32**, 148–157 (2011).
- Kulagowski, J. J., Broughton, H. B., Curtis, N. R., Mawer, I. M., Ridgill, M. P., Baker, R., Emms, F., Freedman, S. B., Marwood, R., Patel, S., Patel, S., Ragan, C. I. & Leeson, P. D. 3-((4-(4-Chlorophenyl)piperazin-1-yl)-methyl)-1H-pyrrolo-2,3-b-pyridine: an antagonist with high affinity and selectivity for the human dopamine D4 receptor. *Journal of medicinal chemistry* **39**, 1941–1942 (1996).
- Haubmann, C., Hübner, H. & Gmeiner, P. 2,2-Dicyanovinyl as a nonaromatic aryl bioisostere: synthesis, binding experiments and SAR studies of highly selective dopamine D4 receptor ligands. *Bioorg Med Chem Lett* **9**, 1969–1972 (1999).

39. Dorsch, S., Klotz, K.-N., Engelhardt, S., Lohse, M. J. & Bünemann, M. Analysis of receptor oligomerization by FRAP microscopy. *Nat Meth* **6**, 225–230 (2009).
40. Aslanoglou, D., Alvarez-Curto, E., Marsango, S. & Milligan, G. Distinct Agonist Regulation of Muscarinic Acetylcholine M2-M3 Heteromers and Their Corresponding Homomers. *J Biol Chem* **290**, 14785–14796 (2015).
41. Bellot, M., Galandrin, S., Boullaran, C., Matthies, H. J., Despas, F., Denis, C., Javitch, J., Mazères, S., Sanni, S. J., Pons, V., Seguelas, M.-H., Hansen, J. L., Pathak, A., Galli, A., Sénard, J.-M. & Galés, C. Dual agonist occupancy of AT1-R- α 2C-AR heterodimers results in atypical Gs-PKA signaling. *Nature chemical biology* **11**, 271–279 (2015).
42. Abbe, E. Beiträge zur Theorie des Mikroskops und der mikroskopischen Wahrnehmung. *Archiv f mikrosk Anatomie* **9**, 413–418 (1873).
43. Hell, S. W. Microscopy and its focal switch. *Nat Meth* **6**, 24–32 (2009).
44. Huang, B., Bates, M. & Zhuang, X. W. Super-Resolution Fluorescence Microscopy. *Annu Rev Biochem* **78**, 993–1016 (2009).
45. Weisenburger, S. & Sandoghdar, V. Light microscopy: an ongoing contemporary revolution. *Contemp Phys* **56**, 123–143 (2015).
46. Moerner, W. E. & Orrit, M. Illuminating single molecules in condensed matter. *Science* **283**, 1670–1676 (1999).
47. Pettersen, E. F., Goddard, T. D., Huang, C. C., Couch, G. S., Greenblatt, D. M., Meng, E. C. & Ferrin, T. E. UCSF Chimera—a visualization system for exploratory research and analysis. *J Comput Chem* **25**, 1605–1612 (2004).
48. Hayes, G., Biden, T. J., Selbie, L. A. & Shine, J. Structural subtypes of the dopamine D2 receptor are functionally distinct: expression of the cloned D2A and D2B subtypes in a heterologous cell line. *Mol Endocrinol* **6**, 920–926 (1992).
49. Sokoloff, P., Giros, B., Martres, M. P., Bouthenet, M. L. & Schwartz, J. C. Molecular cloning and characterization of a novel dopamine receptor (D3) as a target for neuroleptics. *Nature* **347**, 146–151 (1990).
50. Tschammer, N., Elsner, J., Goetz, A., Ehrlich, K., Schuster, S., Ruberg, M., Kühhorn, J., Thompson, D., Whistler, J., Hübner, H. & Gmeiner, P. Highly potent 5-aminotetrahydropyrazolopyridines: enantioselective dopamine D3 receptor binding, functional selectivity, and analysis of receptor-ligand interactions. *Journal of medicinal chemistry* **54**, 2477–2491 (2011).
51. Lowry, O. H., Rosebrough, N. J., Farr, A. L. & Randall, R. J. Protein measurement with the Folin phenol reagent. *J Biol Chem* **193**, 265–275 (1951).
52. Hübner, H., Haubmann, C., Utz, W. & Gmeiner, P. Conjugated Enynes as Nonaromatic Catechol Bioisosteres: Synthesis, Binding Experiments, and Computational Studies of Novel Dopamine Receptor Agonists Recognizing Preferentially the D3 Subtype. *Journal of medicinal chemistry* **43**, 756–762 (2000).
53. Cheng, Y. & Prusoff, W. H. Relationship between the inhibition constant (K1) and the concentration of inhibitor which causes 50 per cent inhibition (I50) of an enzymatic reaction. *Biochem Pharmacol* **22**, 3099–3108 (1973).
54. Chee, M. J. S., Mörl, K., Lindner, D., Merten, N., Zamponi, G. W., Light, P. E., Beck-Sickingler, A. G. & Colmers, W. F. The third intracellular loop stabilizes the inactive state of the neuropeptide Y1 receptor. *J Biol Chem* **283**, 33337–33346 (2008).
55. Kruse, A. C., Ring, A. M., Manglik, A., Hu, J., Hu, K., Eitel, K., Hubner, H., Pardon, E., Valant, C., Sexton, P. M., Christopoulos, A., Felder, C. C., Gmeiner, P., Steyaert, J., Weis, W. L., Garcia, K. C., Wess, J. & Kobilka, B. K. Activation and allosteric modulation of a muscarinic acetylcholine receptor. *Nature* **504**, 101–106 (2013).
56. Mashanov, G. I., Tacon, D., Knight, A. E., Peckham, M. & Molloy, J. E. Visualizing single molecules inside living cells using total internal reflection fluorescence microscopy. *Methods* **29**, 142–152 (2003).
57. Mashanov, G. I., Nobles, M., Harmer, S. C., Molloy, J. E. & Tinker, A. Direct observation of individual KCNQ1 potassium channels reveals their distinctive diffusive behavior. *J Biol Chem* **285**, 3664–3675 (2010).
58. Mashanov, G. I. & Molloy, J. E. Automatic detection of single fluorophores in live cells. *Biophys J* **92**, 2199–2211 (2007).
59. Rosten, E., Jones, G. E. & Cox, S. ImageJ plug-in for Bayesian analysis of blinking and bleaching. *Nat Meth* **10**, 97–98 (2013).
60. Mattila, P. K. & Lappalainen, P. Filopodia: molecular architecture and cellular functions. *Nature reviews Molecular cell biology* **9**, 446–454 (2008).
61. Hiller, C., Kling, R. C., Heinemann, F. W., Meyer, K., Hubner, H. & Gmeiner, P. Functionally selective dopamine D2/D3 receptor agonists comprising an enyne moiety. *Journal of medicinal chemistry* **56**, 5130–5141 (2013).
62. Guex, N. & Peitsch, M. C. SWISS-MODEL and the Swiss-PdbViewer: An environment for comparative protein modeling. *Electrophoresis* **18**, 2714–2723 (1997).
63. Huang, J., Chen, S., Zhang, J. J. & Huang, X.-Y. Crystal structure of oligomeric β 1-adrenergic G protein-coupled receptors in ligand-free basal state. *Nat Struct Mol Biol* **20**, 419–425 (2013).

Acknowledgements

This work was supported by the German Research Foundation (DFG 13/8-2) and by the Francis Crick Institute which receives its core funding from Cancer Research UK (FC001119), the UK Medical Research Council (FC001119), and the Wellcome Trust (FC001119).

Author Contributions

A.T. designed, conducted and analyzed the TIRF experiments, did sample preparation for cryogenic localization microscopy and wrote the manuscript. A.B. and N.P. synthesized the compounds. J.M.K. performed molecular modeling studies. H.H., T.W.G., J.K. and N.T. designed experiments. N.J.M.B. and G.I.M. supervised the analysis of the TIRF experiments and edited the manuscript. S.W. and V.S. designed and conducted cryogenic localization microscopy experiments and wrote the manuscript. L.W. conducted cryogenic localization microscopy studies. P.G. was responsible for the overall project strategy, provided project supervision and wrote the manuscript.

Additional Information

Supplementary information accompanies this paper at <http://www.nature.com/srep>

Competing financial interests: The authors declare no competing financial interests.

How to cite this article: Tabor, A. *et al.* Visualization and ligand-induced modulation of dopamine receptor dimerization at the single molecule level. *Sci. Rep.* **6**, 33233; doi: 10.1038/srep33233 (2016).



This work is licensed under a Creative Commons Attribution 4.0 International License. The images or other third party material in this article are included in the article's Creative Commons license, unless indicated otherwise in the credit line; if the material is not included under the Creative Commons license, users will need to obtain permission from the license holder to reproduce the material. To view a copy of this license, visit <http://creativecommons.org/licenses/by/4.0/>